NASA Technical Paper 1845

Mean-Flow and Turbulence Measurement in the Vicinity of the Trailing Edge of an NACA 63_1-012 Airfoil

James C. Yu

MAY 1981

NASA

NASA Technical Paper 1845

Mean-Flow and Turbulence Measurements in the Vicinity of the Trailing Edge of an NACA 63_1-012 Airfoil

James C. Yu
Langley Research Center
Hampton, Virginia

NASA
National Aeronautics
and Space Administration

**Scientific and Technical
Information Branch**

1981

INTRODUCTION

Noise production resulting from the convection of boundary-layer turbulent eddies over the trailing edge of an aircraft wing is regarded as an important source of community noise from airframes (ref. 1). An extensive experiment was conducted (ref. 2) to determine the physical mechanism of this "trailing-edge-noise" generation, using a two-dimensional NACA 63_1-012 airfoil immersed in a uniform stream. The experimental findings indicate that the flow structure of the boundary layer and near wake in the vicinity of the airfoil trailing edge play a central role in noise generation. The peak of the broadband trailing-edge noise that is generated scales with convection speed and boundary-layer thickness. Evidence shows that the intensity of the noise radiated depends on the changes in turbulence and mean-flow properties which occur at the trailing edge. Therefore, there is a need to understand the structure of mean and turbulent flow near the trailing edge in order to shed more light on the trailing-edge-noise production mechanism.

From the aerodynamic point of view, flow near the trailing edge of an airfoil is an important aspect in airfoil design. The trailing-edge flow controls the circulation around the airfoil and, hence, influences the entire flow field. Although detailed flow measurements at low and moderate free-stream Mach numbers are available for the near wake of flat plates (ref. 3) and airfoil cascades (ref. 4), the same is not true for an isolated airfoil. Detailed turbulent-flow measurements in the boundary layer and near wake of an isolated airfoil at low and moderate free-stream Mach numbers have received proper attention only recently (ref. 5).

In support of the present study of airfoil trailing-edge noise, a computational analysis was initiated (ref. 6) to predict the flow-field details near the airfoil trailing edge. The analysis is based on a finite-element formulism. A parabolized form of the Navier-Stokes equations is solved in conjunction with analysis of a two-dimensional, inviscid potential flow. The computation code is initialized with distributions of mean flow and Reynolds stress measured upstream (90-percent chord) of the trailing edge. Detailed flow-field predictions were generated for the NACA 63_1-012 airfoil at zero angle of attack.

The purpose of this paper is to present the flow-field investigation obtained with the two-dimensional NACA 63_1-012 airfoil. Measurements made include profiles of mean streamwise velocity and distribution of Reynolds stress in a region of 20-percent chord centered at the airfoil trailing edge. Both naturally developed and tripped boundary-layer flows were investigated. The Reynolds number based on airfoil chord was 1.25×10^6, and the angle of attack was set at zero. These measurements provide the required flow-field details for understanding the trailing-edge-noise production process and also serve as the data base for validation of the computation code. Comparisons between measured and computed results for the naturally transitioned flow were previously reported in reference 6. The computed results agreed with the measurements reasonably well.

Identification of commercial products in this report is used to adequately describe the model. The identification of these commercial products does not constitute official endorsement, expressed or implied, of such products or manufacturers by the National Aeronautics and Space Administration.

SYMBOLS AND ABBREVIATIONS

c	airfoil chord, m
c_f	local skin-friction coefficient
d	diameter of hot-wire sensor, m
H	shape factor, δ^*/θ
ℓ	length of hot-wire sensor, m
q^2	turbulent-kinetic-energy flux, $(u')^2 + (v')^2$, m^2/s^2
q_t^2	total turbulent-kinetic-energy flux, $(u')^2 + (v')^2 + (w')^2$, m^2/s^2
R_δ	Reynolds number based on boundary-layer thickness
sta	measurement station
U	streamwise (tangential) mean velocity, m/s
U_∞	free-stream velocity, m/s
u'	streamwise, turbulent, root-mean-square velocity, m/s
$-\overline{u'v'}$	Reynolds shear stress, Pa
u_τ	frictional velocity, m/s
u^+	normalized wall velocity, U/u_τ, m/s
v'	transverse, turbulent, root-mean-square velocity, m/s
$w(y^*)$	wake function, $2 \sin^2\left(\frac{\pi}{2} y^*\right)$
w'	spanwise, turbulent, root-mean-square velocity, m/s
x	streamwise distance along chordline, m
y	transverse distance normal to airfoil surface (or normal to wake centerline), m

y^+ normalized transverse distance from wall in wall coordinate, $\frac{u_\tau y}{\nu}$

y^* normalized transverse distance from wall, y/δ

α wake coefficient

δ boundary-layer thickness, m

δ^* boundary-layer displacement thickness, m

θ angle between mean flow and normal vector of wire, deg; and momentum thickness, m

ν kinematic viscosity, m^2/s

$| \; |$ absolute value

Subscript:

max maximum

min minimum

EXPERIMENTAL APPARATUS, INSTRUMENTATION, AND PROCEDURES

The experiment was performed in the Langley Aircraft Noise Reduction Laboratory. The facility is essentially a continuous-flow, open-section, open-circuit wind tunnel in an anechoic chamber. The rectangular nozzle used to generate the flow had exit dimensions of 0.30 m × 0.46 m and an overall, area contraction ratio of 34. Calibration measurements showed that the exit mean flow was uniform within 1.0 percent of the nozzle exit. The streamwise turbulent intensity was less than 0.5 percent at the center of the nozzle exit. Details of the air supply system and the anechoic chamber are available in reference 7.

Airfoil and Test Section

An NACA 63_1-012 symmetrical airfoil with 0.61-m chord and 0.30-m span were used in the experiment. The airfoil was machined from stock aluminum blocks and the cusped trailing edge was made knife sharp. This airfoil is one of two identical airfoils used in a previous experiment (ref. 2) and was instrumented with a number of flush-mounted transducers to measure fluctuating surface pressure.

The test section, which provided the two-dimensional flow for the airfoil, consisted of two parallel sideplates mounted along the short edges of the nozzle. The airfoil was installed between the sideplates with the leading edge at 25-percent chord downstream of the nozzle exit. A schematic of the test setup is given in figure 1(a). The corresponding photograph is shown in figure 1(b). Other details of the test section may be found in reference 2.

Artificial boundary tripping was achieved by gluing a 0.076-mm-diameter steel wire across the entire span of the airfoil at 6-percent chord from the leading edge. To maintain the symmetry of the flow, identical tripping arrangements were used on both surfaces of the airfoil. The purpose of the tripping was to artificially induce boundary-layer transition near the leading edge so that a thicker boundary layer resulted at the trailing edge. The thickened boundary layer was expected to simulate the higher Reynolds flow conditions prevailing over a full-scale aircraft wing.

Hot-Wire Probe and Instrumentation

At the test Reynolds number of the airfoil, the boundary layer was estimated to be of the order of 10 mm. In order to obtain flow details in the wall region, it was necessary to employ a very small x-wire probe so that adequate spatial resolution and close approach to the wall were possible. A special, subminiature x-wire probe was developed for this study. The tungsten wire used had a 2.5-μm diameter, and its length to diameter ratio ℓ/d was about 200. The lateral spacing between the two component wires was 0.50 mm. A schematic drawing and a photograph of the x-wire probe are shown in figure 2. The small metallic pin mounted on the back of the probe body was used as a contact indicator to provide an accurate initial position of the probe in the boundary-layer measurement. The offset distance between the contact point and probe prong, typically about 0.02 mm, was measured with a high-power microscope. Most measurements were made with the special x-wire probe. Some measurements, however, were made with standard DISA[1] 55P63 x-wire and 55P14 single-wire probes. Both probes use 5-μm platinum-plated tungsten wire with $\ell/d = 250$. Measurements made by the three probes agreed within 5 percent for mean velocity and Reynolds stress. Two channels of hot-wire instrumentation were used for the measurements. Each channel consists of a constant-temperature hot-wire anemometer with a 5:1 bridge, a polynomial linearizer, and a filter.

The hot-wire probe was traversed in a direction normal to the airfoil surface at different chordwise stations. Most of the traverses were made in the midspan plane of the airfoil, although some traverses were also made at different spanwise stations to check the two-dimensionality of the flow. The major component of the traverse rig was a remotely controlled traversing mechanism driven by a stepper motor and a sweep drive unit. The resolution of the traverse was 0.02 mm. During the measurement, the traverse was moved in discrete steps. The size of the steps was varied depending on the probe location, fine step size being used in the flow region near the wall and coarse steps in the outer region of the boundary layer. Typically, 100 data points were obtained in a flow region of one boundary-layer thickness.

Hot-wire probes were calibrated with a free-jet calibration apparatus. The overheat ratio used was about 0.8. For x-wire probes, each component wire was calibrated with the wire normal to the flow. Typically, 12 calibration points were sufficient to accurately define the wire response within the measurement range (0 to 35 m/s). The calibration data were then curve fitted to a fourth

---

[1]Disa Electronics, division of Disamatic, Inc.

degree polynomial by the method of least squares. The coefficients of the polynomial were used to set the linearizer. The inclination angle of the wire with respect to the true probe axis was also calibrated and was found to be within 2° of the desired 45° angle for all x-wire probes. A typical angular response of a component wire is shown in figure 3. The measured response is compared with the law of cosines which is normally assumed for the angular response of an inclined wire. It is seen that the measured response closely follows the law of cosines. The variation from the law of cosines is within 2 percent for θ between 0° and 70°. This means that, if the x-wire is aligned symmetrically to the mean flow, a maximum measurement error of 4 percent could result if the instantaneous-flow incidence angle is within $\pm 25^{\circ}$ of the true probe axis. This maximum error would occur if the root-mean-square flow fluctuation is about 45 percent of the mean velocity. Based on Klebanoff's measurement (ref. 8) in the wall region of the turbulent boundary layer over a smooth flat plate, flow fluctuations of this magnitude occur only when $y^{+} = u_{\tau}y/\nu$ is less than 30. For the present study, the closest approach to the wall for x-probes was about $y^{+} = 40$. Therefore, the departure of the wire response from the law of cosines was not considered significant. By use of the x-wire probe calibration procedure just discussed, the velocity measured by the x-wire and single-wire probes is compared with that obtained with a pitot tube on the centerline of the calibrator nozzle. (See fig. 4.) Over most of the measurement range, x-wire results are within 5 percent of the pitot-tube measurements. For the single wire, the agreement was within 1 percent.

One of the major problems in the interpretation of hot-wire signals is that they are sensitive to variations of mean-flow temperature. In the present experiment, the actual drift of mean-flow temperature during the measurement was small (within $1^{\circ}C$). The problem encountered was that the temperature of the flow in which the probe was calibrated differed from that of the flow being measured. Since probes were always calibrated just prior to the measurement, this temperature difference never exceeds $5^{\circ}C$. Therefore, a correction method developed by Bearman (ref. 9), suitable for correcting bridge voltage with small, mean-flow temperature changes, was used. This correction method was checked with the calibration data obtained at several different mean-flow temperatures. The accuracy of the method was found to be within 1 percent, a conclusion that was also reached by Bearman. If mean-flow temperature differs during the measurement from that used at calibration, Bearman's method is used to compute the full-scale flow voltage at $\theta = 0^{\circ}$. The bridge voltage at maximum mean velocity for $\theta = 0^{\circ}$ is required in order to span the linearizer.

Data Reduction

Mean velocities and Reynolds stresses of the flow were deduced from suitably amplified and linearized signals obtained from two hot-wire channels via a digital computer. Instantaneous signals were first digitized at a rate of 100 kHz, and then the axial and transverse components were obtained by adding and subtracting the two signals, respectively, at each probe location by assuming a cosine-law angular response. The mean and mean-square flow quantities were computed by continuous ensemble averaging over the data blocks. The data acquisition at each probe position terminates when both the mean and mean-square values converged within specified tolerances or when the maximum allowed number

of averages was exceeded. In the latter situation, the probe position was flagged and the deviation from the mean recorded. The measurement was repeated when more than 10 percent of the data points were flagged. The tolerance for convergence for mean velocity was 1 percent and for root-mean-square turbulence quantities was 2 percent. For mean velocity measurements, all data satisfies the convergence criteria. For fluctuating quantities in a typical probe traverse, convergence was usually met for 95 percent of the data points.

Experimental Procedures

For each test run, the tunnel flow was first stabilized at 30.5 m/s. The hot-wire probe was then moved to the uniform-flow region away from the airfoil. With the probe properly aligned to the flow, the cold resistance was measured. The flow temperature deduced from measured cold resistance was used to compute bridge voltage corresponding to maximum flow velocity. For a single-wire probe, the same voltage at $\theta = 0^{\circ}$ could be measured directly. A comparison between the computed voltage and the directly measured value thus served as an independent check for the probe alignment. With an x-wire probe, it was not convenient to align each wire normal ($\theta = 0^{\circ}$) to the test flow. For the procedure used, the bridge output voltages were measured with the probe aligned to the flow ($\theta = 45^{\circ}$). The computed voltages at $\theta = 45^{\circ}$ were compared to the measured values as a check of probe alignment. The required, full-scale, flow-bridge output voltage at $\theta = 0^{\circ}$ can be obtained either from Bearman's method or from the directional response of the wire. The two usually agreed within 2 percent.

For each boundary-layer traverse, the probe axis was aligned tangential to the airfoil surface at the initial position of the traverse by use of a high-power telescope with a resolving power of 0.01 mm. The precise location of the probe, however, was provided by the contact pin arrangement discussed earlier. The probe was traversed in a direction normal to the airfoil surface in the midspan plane of the airfoil. For wake measurements, the probe was aligned tangential to the chordline of the airfoil.

RESULTS AND DISCUSSION

Verification of Measurement Technique

Since x-wire measurements are subject to more sources of experimental error (such as probe orientation, probe geometry, wall proximity interference, and mismatching of two component wires) than the single-wire measurements, a comparison between corresponding measurements obtained by the two different types of probes is indicative of the reliability of the present measurement. Shown in figure 5 are comparisons of normalized, streamwise, mean velocity U/U_{∞} for the naturally developed boundary layer and for the artifically tripped boundary layer. It is seen that the agreement is very good, within 5 percent. The comparison shown in figure 6 is of normalized, streamwise, root-mean-square (rms) turbulent velocity u'/U_{∞} measured from the x-probe and the rms fluctuating velocity measured by the single-wire probe. It should be noted that, for a single wire which responds to velocity normal to the wire, the measured results are expected to be higher than the true u' because of strong lateral and

transverse velocity fluctuations. Bradshaw (ref. 10) discussed in detail the single-wire response in a turbulent boundary layer. For a turbulent boundary layer over a smooth flat plate, he estimated the maximum error for single-wire measurement of u' to be 2 percent. The actual error depends on the probe location in the boundary layer and the turbulence structure of the flow. From figure 6, it is seen that the single-wire result is about 7 percent higher than the x-wire result, suggesting a 5-percent measurement error with the x-wire probe. Hence, the maximum measurement error on Reynolds shear stress $-\overline{u'v'}$ could approach 10 percent.

The symmetry of the test flow was deduced from flow measurements made in the near wake of the airfoil. Shown in figure 7 are U and $-\overline{u'v'}$ distributions across the airfoil near the wake at $x/c = 1.0029$. The symmetry is within 2 percent for both U and $-\overline{u'v'}$. Selected traverses made across the entire wake flow at downstream stations indicated similar results. Thus, most of the wake traverses were made on the same side where the boundary-layer measurements were performed.

Determination of Mean-Flow-Integral Properties

To determine the boundary-layer mean-flow-integral properties c_f and δ, the measured velocity profiles were curve fitted (least-square method) to the wall-wake law as proposed by Coles (ref. 11):

$$u^+ = \frac{1}{0.41} \ln y^+ + 5 + \frac{\alpha}{0.41} w(y^*) \tag{1}$$

where the wake function (law of the wake) $w(y^*)$ is given by

$$w(y^*) = 2 \sin^2 \left(\frac{\pi}{2} y^* \right) \tag{2}$$

The three parameters u_τ, α, and δ are determined from the fitting procedure. Shown in figure 8 are typical comparisons between the measurement and Coles' law of the wall,

$$u^+ = \frac{1}{0.41} \ln y^+ + 5 \tag{3}$$

It is seen that for both tripped and untripped boundary layers, the agreement is very good beyond transition in the near-wall region ($30 < y^+ < 300$). In the outer flow region, the measurement deviates from the wall law, more so for the

tripped than the untripped boundary layer. This indicates that artificial tripping increases the wake component in the boundary layer. The corresponding comparison with the wake law is given in figure 9. Agreement between the data and Coles' wake function is fair for the tripped boundary layer but rather poor for the untripped boundary layer, presumably because of the lack of wake components in the untripped boundary layer.

The local skin-friction coefficient c_f was computed from u_τ and U_∞ by

$$c_f = 2\left(\frac{u_\tau}{U_\infty}\right)^2 \tag{4}$$

The momentum thickness θ and displacement thickness δ^* for the wake flow were obtained by integrating the measured velocity profiles in y using a Runge-Kutta third-order numerical scheme. Since measurements cannot be obtained for $y^+ < 40$, direct integration over only the measured velocity can introduce large errors in θ and δ^* for boundary-layer flow. This is because the velocity distribution near the wall ($y^+ < 40$) has the greatest contribution to the integrals of θ and δ^*. In view of the good fit for the present measurements obtained with Coles' law of the wall, the mean velocity was extrapolated to the wall through Coles' law (eq. (3)) and the linear law given by

$$u^+ = y^+ \tag{5}$$

The two flow regions intersect at $y_o^+ \cong 10.8$. The velocity extrapolation was done with equation (5) from the wall to y_o^+ and with equation (3) from y_o^+ to $y^+ \cong 40$. Although the transitional behavior from linear region to log region is not taken into account in the extrapolation, it is felt that the θ and δ^* obtained with this extrapolation should be much closer to the true values than otherwise. The improvements obtained with this extrapolation for the untripped flow were about 15 to 20 percent in θ and 25 to 30 percent in δ^*. For the tripped flow, the improvements were about half of those given above.

Measured flow properties for both naturally developed flow and artificially tripped flow are presented in the following sections. Mean velocity and rms turbulent velocities u' and v' are normalized to free-stream velocity. Reynolds shear stress $-\overline{u'v'}$ and turbulent kinetic energy flux q^2 are normalized to the square of free-stream velocity. Also presented are the turbulent-shear correlation coefficient $-\overline{u'v'}/u'v'$ and the ratio of Reynolds shear stress to turbulent kinetic-energy flux $|\overline{u'v'}|/q^2$.

Naturally Developed Flow

The development of streamwise mean velocity for the untripped flow is given in figure 10, over the flow region $0.9 \leqq x/c \leqq 1.1$. The chordwise locations of the measurement stations are given in table 1. For boundary-layer flow

($x/c < 1.0$), the mean velocity profiles are similar. By proper integration and/or fitting with Coles' wall-wake law, integral properties δ^*, θ, H, and c_f were obtained from these mean velocity profiles. Results are given in figure 11. Both δ^* and θ are essentially constant at 1 mm and 1.4 mm, respectively, in the boundary layer, with a slight initial increase at $x/c \cong 0.94$. In the near wake, both quantities exhibit maxima of about 1.1 mm and 1.5 mm, respectively, at $x/c \cong 1.005$. The shape factor H is nearly constant ($\cong 1.39$) in the boundary layer. Downstream of the trailing edge, H is seen to exhibit an initial sudden reduction (to about 1.3), followed by a gradual decrease towards unity as expected for the far wake. The local skin-friction coefficient c_f exhibits some scatter. The general trend is a slight reduction of skin friction as the airfoil trailing edge is approached. The average value of c_f is about 0.0039 over the last 10 percent of the airfoil chord.

Distributions of u', v', $-\overline{u'v'}$, and q^2 are presented in figures 12 to 15. The peak, streamwise, turbulent intensity u'/U_∞ is about 7.5 percent in the boundary layer and increases to about 8.0 percent just downstream of the trailing edge. This is followed by a gradual decay farther downstream. Also noted is a spike in u'/U_∞ in the slipstream where the two boundary layers from opposite sides of the airfoil meet. This spike migrates outward and merges with the broader peak observed in the boundary-layer region. The position of the broad peak in u' is found to progressively move away from the chordline indicative of the spreading of the mixing region in the wake, as shown in figures 12(a) and 12(b). The transverse turbulent intensity v'/U_∞ has a peak value of 6 percent at $x/c = 0.9$. The peak value occurs very close to the surface and decays continuously with downstream location in the wake. Of particular interest is the reduction in v'/U_∞ across the trailing edge. (Compare sta 11 with sta 12 in fig. 13.) At $x/c = 1.1$, the peak value is reduced to about 3.5 percent. The distribution for v' exhibits a spike in the slip stream similar to the u' distribution. This spike, however, remains on the chordline of the airfoil and decays gradually with downstream distance. Hence, the peak value of v'/U_∞ in the near wake remains on the chordline.

Distribution of the Reynolds shear stress is given in figure 14. At $x/c = 0.9$, the normalized, peak shear stress is about 0.0012. The peak value then increases rapidly to 0.0017 at $x/c = 0.9583$, followed by a decay to its initial value at $x/c = 0.9896$. From $x/c = 0.9896$, the peak value of the normalized shear stress decreases. In the slipstream, a spike is also observed. The spike diffuses outward and eventually merges with the broad peak in the outer region into a smooth distribution. The diffusion of the slipstream spike for $-\overline{u'v'}$ is seen to be similar to that for u'. From boundary layer to the near wake, the Reynolds shear stress shows a reduction which occurs immediately downstream of the trailing edge.

Distributions of turbulent-kinetic-energy flux q^2 are shown in figure 15. It should be noted that the q^2 defined here is not the total turbulent-kinetic-energy flux, because the spanwise velocity fluctuation w' was not measured. An estimate of the total turbulent-kinetic-energy flux ($q_t^2 = u'^2 + v'^2 + w'^2$) may be obtained if it is assumed that $w'^2 = 0.5(u'^2 + v'^2)$, as was done in reference 5. In that case, $q_t^2 = 1.5q^2$ and the total turbulent-kinetic-

energy flux q_t^2 would be 50 percent higher than the value of q^2 plotted. As shown in figure 15, q^2 remains nearly constant for the four initial measurement stations ($0.9 \leq x/c \leq 0.9688$) with $q^2/U_\infty^2 \cong 0.09$. From $x/c = 0.9688$ to $x/c \cong 1$, a gradual decrease in q^2 is noted with $q^2/U_\infty^2 \cong 0.07$ at the trailing edge. For all boundary-layer stations, q^2 peaks very close to the airfoil surface. In the near-wake region, note that a high q^2 concentration occurs in the slipstream. The effects of the lateral turbulence mixing in the wake region, however, diffuses this high concentration of turbulent kinetic energy over a distance of about 6-percent chord. At $x/c = 1.1$, the location of maximum q^2 is seen to be displaced to the middle of the wake mixing layer.

The distribution of turbulent-shear correlation coefficient is shown in figure 16. This is obtained by dividing the measured Reynolds shear stress $-\overline{u'v'}$ by the product of the root-mean-square values of u' and v'. The correlation coefficient distribution measured in the boundary-layer flow typically has a positive maximum near the airfoil surface and remains nearly constant at the maximum value for the inner part of the boundary layer. As the outer edge of the boundary layer is approached, the correlation coefficient drops rapidly to zero. If the boundary-layer flow is generated by a very low, turbulent, uniform free-stream flow, the correlation coefficient should remain nearly zero outside the boundary layer. In the present experiment, the free-stream flow was provided by the potential core of a free jet. At the airfoil trailing edge, the thickness of the free-jet shear layer was about 7.6 cm and the distance from the airfoil trailing edge to the inner edge of the free-jet shear layer is about 11.4 cm. Even though the turbulence intensities u' and v' and Reynolds shear stress $-\overline{u'v'}$ measured in the free-stream of the airfoil are extremely low (see figs. 12 to 14), the distribution of correlation coefficient in figure 16 reveals the presence of the free-jet shear layer. This is indicated by the reversal of the sign of the correlation coefficient as the measurement is made farther away from the outer edge of the boundary layer in the free-stream flow.

Similar observations can also be made in the near-wake region of the airfoil. It is pertinent to note at this point that, although the distribution of the correlation coefficient reveals the presence of the free-jet shear layer, the magnitudes of u', v', and $-\overline{u'v'}$ are extremely low and would not affect the validity of the same measurements made inside the boundary layer. The maximum value of the correlation coefficient varies from 0.25 at $x/c = 0.9$ to 0.4 at the trailing edge. In the near-wake region, a further increase is noted and a value of about 0.5 for the correlation coefficient is reached at $x/c = 1.1$. Comparing the shear correlation across the trailing edge (sta 11 and sta 12 in fig. 16), it is seen that the shear-correlation profile displaces away from the chordline in the near wake. Depending on the Reynolds number based on δ, correlation coefficients of about 0.5 have been observed in a fully developed, turbulent boundary layer over a flat plate under zero pressure gradient (ref. 8) and in a fully developed, turbulent, two-dimensional channel flow (ref. 12). The fact that there exists a region near the wall over which the correlation coefficient remains nearly constant is indicative of the presence of a constant stress layer as expected from theoretical arguments (ref. 13). In the near-wake region, the extent of the constant-stress region is seen to broaden with downstream distance and is further displaced from the chordline of the airfoil.

Figure 17 is an illustration of the distribution of $|\overline{u'v'}|/q^2$. This ratio is a measure of the relative importance of turbulent-kinetic-energy production in the flow and the turbulent-kinetic-energy content in the flow. For most turbulent boundary layers, the ratio is nearly a constant in the outer region of the boundary layer. For example, the ratio is about 0.167 for a turbulent boundary layer over a flat plate under zero pressure gradient (ref. 14). For the present airfoil, there are indications in figure 17 that $|\overline{u'v'}|/q^2$ in the boundary layer takes on a value of 0.13 at $x/c = 0.9$, increases to a maximum of 0.20 at $x/c = 0.9844$, and then decreases to 0.18 at the trailing edge. In the near wake, an initial decrease is noted just downstream of the trailing edge with $|\overline{u'v'}|/q^2 = 0.18$, followed by a rather gradual increase to $|\overline{u'v'}|/q^2 = 0.2$ at $x/c = 1.1$. Since the value of q^2 used is just the sum of mean squares of the streamwise and transverse velocity fluctuations, it represents only 2/3 of the total turbulent kinetic energy q_t^2. Thus, $|\overline{u'v'}|/q_t^2$ would be about 0.13, a value somewhat lower than that established for a flat-plate turbulent boundary layer.

It is also interesting to note that the region over which $|\overline{u'v'}|/q^2$ is constant exists only over a limited extent in the boundary layer. The sharp drop-off of this ratio in the outer region of the boundary layer is also not observed for a flat-plate turbulent boundary layer. In the near wake, however, $|\overline{u'v'}|/q^2$ is nearly constant over most of the outer region of the wake and decreases sharply to zero near the centerline of the wake. The nonzero value of $|\overline{u'v'}|/q^2$ observed in the free-stream flow is due to the influence of the free-jet shear layer as discussed earlier. It should be noted, however, that $|\overline{u'v'}|$ and q^2 are extremely low in the free stream.

In regard to the dependence of trailing-edge-noise production on the boundary-layer/near-wake turbulence properties near the edge, it has been observed for the untripped flow that u' increases just downstream of the trailing edge while v' and $-\overline{u'v'}$ decrease and the shear correlation profile displaces away from the chordline. These observations support the contention made in reference 2 that the coherent eddies undergo an adjustment across the trailing edge in the process of producing trailing-edge noise.

Artificially Tripped Flow

In the second part of the investigation, the boundary-layer growth along the airfoil was enhanced by artificial tripping. Distributions of streamwise mean velocity are given in figure 18. It is seen that the boundary layer is thickened by the leading-edge tripping (compare fig. 18 with fig. 10). The U/U_∞ profiles are nearly identical in the boundary layer and also in the outer part of the wake. This is indicative of the establishment of a fully developed, equilibrium, boundary-layer flow near the airfoil trailing edge. The integral mean-flow properties deduced from the U distributions are presented in figure 19. At the first measurement station ($x/c = 0.9$) in the boundary layer, the values of θ and δ^* are 1.87 mm and 2.95 mm, respectively. The boundary-layer displacement thickness δ^* exhibits an initial increase, reaching a maximum value of 3.05 mm at $x/c \cong 0.98$, followed by a reduction towards the trailing edge. Similar behavior is noted for θ. Both θ and δ^* are seen to increase to a maximum value just downstream of the trailing edge at $x/c = 1.005$,

similar to the untripped flow. This behavior is believed to be typical of flow transition from bounded, boundary-layer shear flow to free-shear, near-wake flow. The shape factor was reasonably constant at 1.55 at initial measurement locations from $x/c = 0.9$ to $x/c = 0.98$. Close to the trailing edge, H starts to decrease, reaching a value of 1.51 at $x/c \cong 0.995$. This decrease continues into the near wake and tends to approach unity asymptotically, as expected, for the far wake. The major difference noted in the mean-flow integral properties between the tripped and untripped boundary layers lies in the local skin-friction coefficient. While a slight decrease of c_f is noted towards the trailing edge of the untripped flow, the tripped boundary layer indicates a definitive opposite trend. The averaged values of c_f over the last 10-percent of airfoil chord are 0.0025 and 0.0039 for the tripped and untripped boundary layer, respectively.

The distributions of u'/U_∞ and v'/U_∞ are given in figures 20 and 21, respectively. The u'/U_∞ distributions measured in the boundary layer are similar. The common peak value is about 7 percent, which occurs at $y/\delta^* \cong 1.3$. In the near-wake region, the outer part of the u'/U_∞ distributions are also nearly identical to that measured in the boundary layer. In the slipstream downstream of the trailing edge, a hump appears, as previously occurred for the untripped flow. The lateral diffusion of the hump, however, is more rapid than for the untripped case. Measured v'/U_∞ distributions show trends similar to those for the u'/U_∞ variation. The peak value in the boundary layer and the outer part of the wake is about 5.5 percent. The general behavior of the slipstream spike in the wake region is similar to that noted for the untripped flow. Contrary to the untripped flow, there is no change observed in u' or v' across the trailing edge other than the spikes in the slipstream.

Distributions of Reynolds shear stress and turbulent kinetic energy for the tripped flow are presented in figures 22 and 23, respectively. Similar distributions of $-\overline{u'v'}/U_\infty^2$ are noted in the boundary-layer region with a peak value of 0.0014. A slight increase in the peak value is found in the initial part of the measurement region ($x/c \cong 0.9$). Downstream of the airfoil trailing edge, the peak value of $-\overline{u'v'}/U_\infty^2$ increases to 0.0017 and remains at this value to $x/c = 1.02$ followed by a decay to 0.0012 at $x/c = 1.1$. The variation of q^2/U_∞^2 is similar to that of the Reynolds shear stress. The peak value is about 0.008 which occurs at 0.3δ from the airfoil surface. In comparison with corresponding measurements made for the untripped flow, it is seen that the peak values are comparable for the two flows, but the tripping displaces the region of maximum, turbulent kinetic energy farther away from the surface. In the near-wake region, the q^2/U_∞^2 distribution in the outer part of the wake is again similar to those measured in the boundary layer. A decrease of turbulent kinetic energy is seen to occur for $x/c > 1.06$. The high level of q^2 in the slipstream is seen to diffuse more rapidly for the tripped flow than that for the untripped flow.

Shown in figure 24 is the distribution of turbulent-shear correlation coefficient and in figure 25 is the ratio of turbulent energy production and turbulent kinetic energy. The turbulent shear correlation remains nearly constant in the boundary-layer region. The maximum value of $-\overline{u'v'}/u'v'$ is about 0.32. A slight increase in turbulent shear correlation may be noted from $x/c = 0.9$ to $x/c = 0.9417$. In the wake region, the maximum value of the

correlation coefficient is about 0.38, and a slight decrease is noted at $x/c = 1.1$. In comparison with the corresponding measurements made in the untripped flow, it is seen that the effect of tripping is the elimination of most of the streamwise variations of the shear correlation coefficient. Moreover, $-\overline{u'v'}/u'v'$ is seen to maintain a constant value over most parts of the boundary layer and/or wake for the tripped flow. On the other hand, tripping reduces the magnitude of the correlation coefficient. The ratio of Reynolds shear stress $|\overline{u'v'}|$ and the turbulent kinetic energy q^2 (see fig. 24) is seen to follow a behavior similar to that noted for the shear correlation coefficient. The ratio $|\overline{u'v'}|/q^2$ remains nearly constant over most parts of the boundary layer and/or wake with very little streamwise variation. In the boundary layer, the ratio is about 0.16, and in the wake, it is about 0.18. Both values are lower than those found for the naturally developed flow. The influence of the free-jet shear layer can be inferred from the $-\overline{u'v'}/u'v'$ and $|\overline{u'v'}|/q^2$ distributions outside the boundary layer and wake flow. As pointed out previously, the magnitudes of $\overline{u'v'}$, u', v', and q^2 are extremely small outside the boundary layer and wake; hence, the existence of the free-jet shear layer does not influence the accuracy of the measurements made in the boundary-layer and wake flows.

Of particular significance, the changes in turbulence properties across the trailing edge for the tripped flow exhibit a different behavior from that observed for the untripped flow. The only change noted for the tripped flow is in the Reynolds shear stress which showed an increase downstream of the trailing edge. As discussed in the previous section, Reynolds shear stress and v', for the untripped flow, were found to decrease in the immediate downstream region of the trailing edge, while u' showed an increase there. These contrasting behaviors are believed to be a result of increased fine-scale turbulence due to tripping as well as a result of loss of correlation of the coherent eddies in the boundary layer. As far as the trailing-edge-noise mechanism is concerned, more refined measurement such as a conditioning sampling technique may be necessary in order to resolve the difference observed between the two types of flow.

Comparison of Present Untripped Results With Measurements of Turbulent Boundary Layer Over a Flat Plate

The flow field around the present airfoil is affected by the streamline curvature and variable pressure gradient. The airfoil surface near the trailing edge ($x/c > 0.9$) is concave, and a mild positive pressure gradient prevails near the trailing-edge region. It is of interest to qualitatively compare the present results for the naturally developed flow with those obtained for turbulent flow over a flat plate with zero pressure gradient. In this way, the influences of mean-flow pressure gradient and streamline curvature on the development of a boundary layer may be delineated.

The mean, streamwise velocity distribution for the present airfoil is seen to obey the law of the wall for $y^+ \leq 300$. (See fig. 8.) In the outer region, a weak wake component is also noted. For a flat-plate boundary layer, the law of the wall generally holds (ref. 13) for y^+ up to 1000. The measured, local

skin-friction coefficient is about 0.0039 for the untripped airfoil as compared to a value of 0.0036 predicted by the empirical formula of Ludweig and Tillmann (see Hinze, ref. 13) for the flat-plate boundary layer

$$c_f = 0.246 \cdot 10^{-0.678H}\left(\frac{U_\infty \theta}{\nu}\right)^{-0.268} \tag{6}$$

valid for $\frac{U_\infty \theta}{\nu}$ from 10^3 to 10^4. The shape factor was deduced from the data to be 1.39 for the untripped-airfoil boundary layer, compared to a value of 1.39 predicted by Hamma's empirical formula (see Hinze, ref. 13) for the flat-plate boundary layer

$$H = \left(1 - 6.3\,\frac{u_\tau}{U_\infty}\right)^{-1} \tag{7}$$

For the turbulent quantities, the present measurements can be compared with those reported by Klebanoff (ref. 8) for a fully developed, turbulent boundary layer over a flat plate. The Reynolds number based on boundary-layer thickness δ was 7.5×10^4 for Klebanoff's data and is 2×10^4 at the trailing edge of the present, naturally developed boundary layer. The value of u'/U_∞ at 0.1δ was about 7.3 percent as determined by Klebanoffs' measurement, compared to a value of 7 percent obtained at the airfoil trailing edge. The ratio v'/U reached a peak of about 4 percent for the flat-plate boundary layer. The airfoil measurements indicate a 5-percent peak near the trailing edge. The normalized Reynolds shear stress $-\overline{u'v'}/U_\infty^2$ and turbulent-shear correlation coefficient $-\overline{u'v'}/u'v'$ were 0.014 and 0.5, respectively, from Klebanoff's measurements. For the airfoil, the corresponding values are 0.017 and 0.4. The ratio $|\overline{u'v'}|/q_t^2$ exhibited a flat peak of 0.166 for the flat plate and 0.13 for the airfoil.

In general, the boundary-layer measurements made near the trailing edge of the untripped airfoil follow closely the trends observed in a flat-plate boundary layer under zero pressure gradient. This observation is indicative of the weak influences of the streamline curvature and the adverse pressure gradient on the airfoil boundary layer. It should be pointed out, however, that the observed variation of flow properties in the flow direction as discussed in Naturally Developed Flow would be absent for a fully developed, turbulent boundary layer over a flat plate.

Effect of Tripping on Airfoil Boundary Layer

As was stated previously, the purpose of boundary-layer tripping is to enhance the flow development and to promote the mixing so that a thicker boundary layer is obtained near the trailing edge. It should be pointed out that

a tripping device such as the one used in the present study, which is common to this type of study, may alter the turbulence structure downstream, as cautioned by Willmarth (ref. 14). This is especially true for large-scale disturbances in the flow. Nevertheless, the thicker boundary layer resulting from the tripping does facilitate measurement and does increase experimental accuracy. In addition, the transition is artificially fixed by the tripping wire, which causes minimization of the nonuniformities in the spanwise direction of the flow. The measurements obtained for the tripped flow are considered representative of those which would exist if an airfoil of longer chord were used.

The most fundamental difference found between the naturally developed flow and the tripped flow is the lack of streamwise variation of the latter. The artificially tripped flow exhibits a high degree of uniformity in all normalized flow properties, both in mean flow and in turbulence quantities. For the mean-flow field, tripping increases the wake component in the outer region, reduces the local skin-friction coefficient, and slightly increases the shape factor. The value of R_δ for the tripped flow is about 5.1×10^4, a factor of 2.5 increase over the untripped flow. Laufer (ref. 12) reported turbulence measurements in a fully developed, turbulent, two-dimensional channel flow where R_δ was varied. His results indicate that, in general, the normalized turbulent quantities reduce as R_δ is increased. Similar findings are obtained in the present measurements. As R_δ is increased by flow tripping, u'/U_∞, v'/U_∞, $-\overline{u'v'}/U_\infty^2$, q^2/U_∞^2, $-\overline{u'v'}/u'v'$, and $|\overline{u'v'}|/q^2$ all show reduction, compared to the untripped flow where R_δ is lower.

The local skin-friction coefficients for both tripped and untripped boundary layers are found to be within 10 percent of the predictions made from Ludweig and Tillmann's empirical formula (eq. (6)), with the predicted values being lower. Although it was found that local distributions for mean or turbulent properties did not collapse for the two types of flow when the transverse coordinate was normalized to δ^*, δ, or θ, similarity is observed for the wake velocity defect. Shown in figure 26 is the distribution of the wake-velocity defect with downstream distance normalized by the momentum thickness measured at the trailing edge. The similarity between the untripped and tripped flows is apparent. The asymptotic behavior of the wake-defect distribution also follows the expected $(x/\theta)^{-0.5}$ variation.

CONCLUDING REMARKS

Measurements of mean and turbulent flow fields have been conducted near the trailing edge of a symmetrical NACA 63_1-012 airfoil at zero angle of attack. The boundary-layer and near-wake characteristics were investigated for both naturally developed flow and artificially tripped flow.

For the naturally developed flow, the general trends observed for the mean and turbulence profiles were found to be similar to those reported for a fully developed, turbulent boundary layer over a flat plate under zero pressure gradient. This suggests that the influences of the mild, adverse pressure gradient and the slight streamline curvature on the airfoil trailing-edge flow are weak.

Notable streamwise variations in turbulence properties were found in the airfoil flow field, however, which are not expected for a fully developed equilibrium flow.

The main effect of artificially tripping the boundary layer near the airfoil leading edge is to make both mean and turbulent profiles nearly independent of streamwise location. The changes observed in the mean- and turbulence-flow properties as a result of tripping are expected on the basis of the Reynolds number based on the boundary-layer thickness. Reductions in skin-friction coefficient, turbulent intensities, Reynolds shear-stress, turbulent kinetic energy, and turbulence shear correlation coefficient occur when Reynolds number based on boundary-layer thickness is increased as a result of tripping.

The changes in the turbulence properties observed for the untripped flow just downstream of the airfoil trailing edge are believed to be manifestations of the adjustment made by the coherent eddies in the boundary layer when encountering the trailing edge. This adjustment governs the production of trailing-edge noise. The fact that most of the observed changes in the turbulence properties for the untripped flow were absent in the tripped flow is believed to be attributable to the increase in fine-scale turbulence and a loss of correlation for the coherent eddies due to tripping.

Langley Research Center
National Aeronautics and Space Administration
Hampton, VA 23665
March 24, 1981

REFERENCES

1. Hardin, Jay C.: Airframe Self-Noise - Four Years of Research. NASA TM X-73908, 1976.

2. Yu, J. C.; and Joshi, M. C.: On Sound Radiation From the Trailing Edge of an Isolated Airfoil in a Uniform Flow. AIAA Paper No. 79-0603, Mar. 1979.

3. Chevray, Rene; and Kovasznay, Leslie S. G.: Turbulence Measurements in the Wake of a Thin Flat Plate. AIAA J., vol. 7, no. 8, Aug. 1969, pp. 1641-1643.

4. Raj, R.; and Lakshminarayana, B.: Characteristics of the Wake Behind a Cascade of Airfoils. J. Fluid Mech., vol. 61, pt. 4, Dec. 18, 1973, pp. 707-730.

5. Viswanath, P. R.; Cleary, J. W.; Seegmiller, H. L.; and Horstman, C. C.: Trailing-Edge Flows at High Reynolds Number. AIAA Paper 79-1503, July 1979.

6. Baker, A. J.; Yu, J. C.; Orzechowski, J. A.; and Gatski, T. B.: Prediction and Measurement of Turbulent Aerodynamic Trailing Edge Flows. AIAA-80-1395, July 1980.

7. Yu, J. C.; and Dixon, N. R.: Experimental Study of Sound Radiation From a Subsonic Jet in Simulated Motion. AIAA J., vol. 18, no. 4, Apr. 1980, pp. 427-433.

8. Klebanoff, P. S.: Characteristics of Turbulence in a Boundary Layer With Zero Pressure Gradient. NACA Rep. 1247, 1955. (Supersedes NACA TN 3178.)

9. Bearman, P. W.: Corrections for the Effect of Ambient Temperature Drift on Hot-Wire Measurements in Incompressible Flow. DISA Information No. 11, May 1971.

10. Bradshaw, P.: An Introduction to Turbulence and Its Measurement. Pergamon Press, Inc., c.1971.

11. Coles, Donald: The Young Person's Guide to the Data. Computation of Turbulent Boundary Layers - 1968 AFOSR-IFP-Stanford Conference, Volume II, D. E. Coles, and E. A. Hirst, eds., Stanford Univ., c.1969, pp. 1-45.

12. Laufer, John: Investigation of Turbulent Flow in a Two-Dimensional Channel. NACA Rep. 1053, 1951. (Supersedes NACA TN 2123.)

13. Hinze, J. O.: Turbulence. Second ed. McGraw-Hill Book Co., c.1975.

14. Willmarth, W. W.: Structure of Turbulence in Boundary Layers. Volume 15 of Advances in Applied Mechanics, Chia-Shun Yih, ed., Academic Press, Inc., 1975, pp. 159-254.

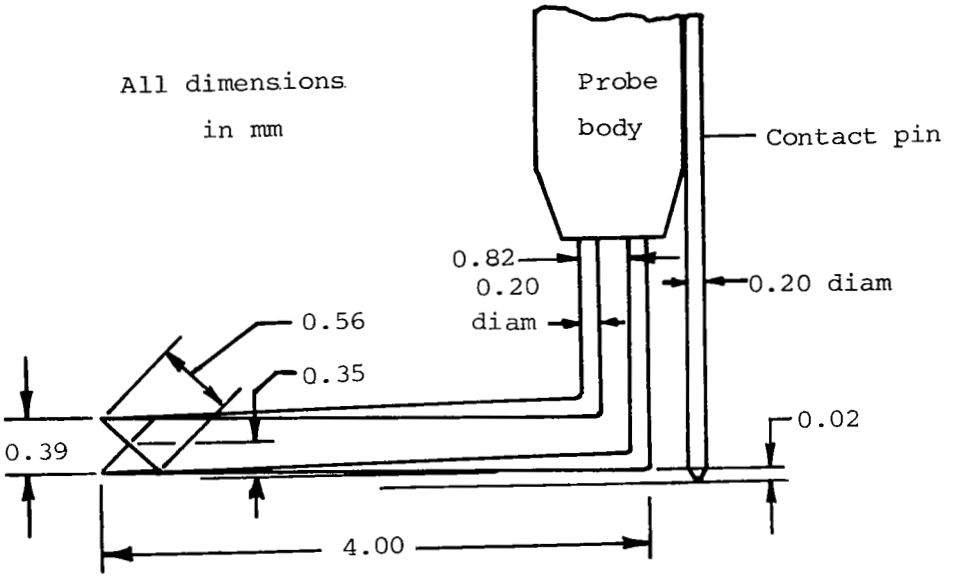

(a) Schematic.

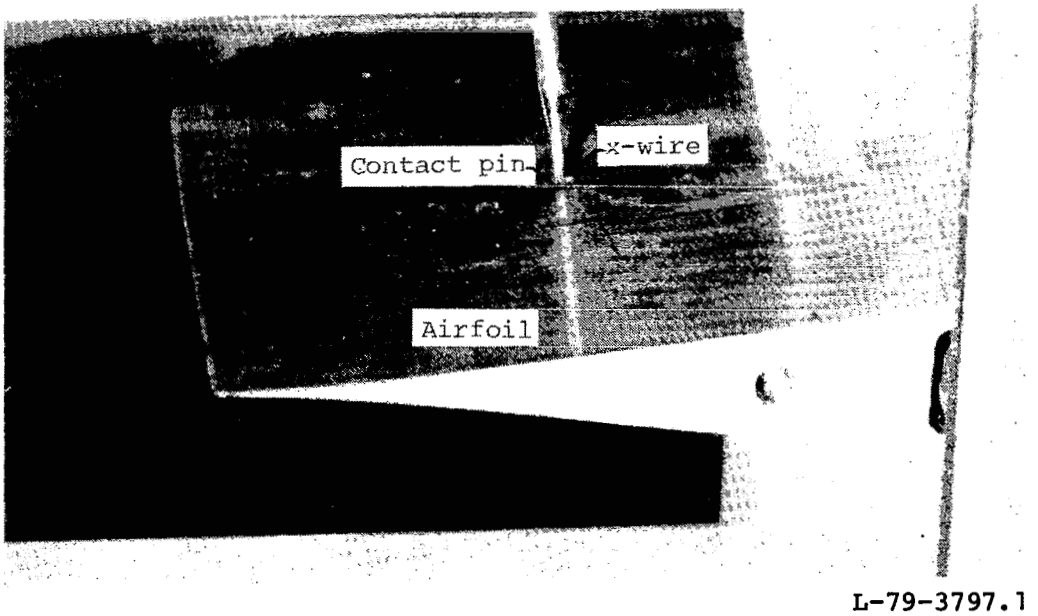

L-79-3797.1

(b) Photograph.

Figure 2.- Details of x-wire probe arrangement.

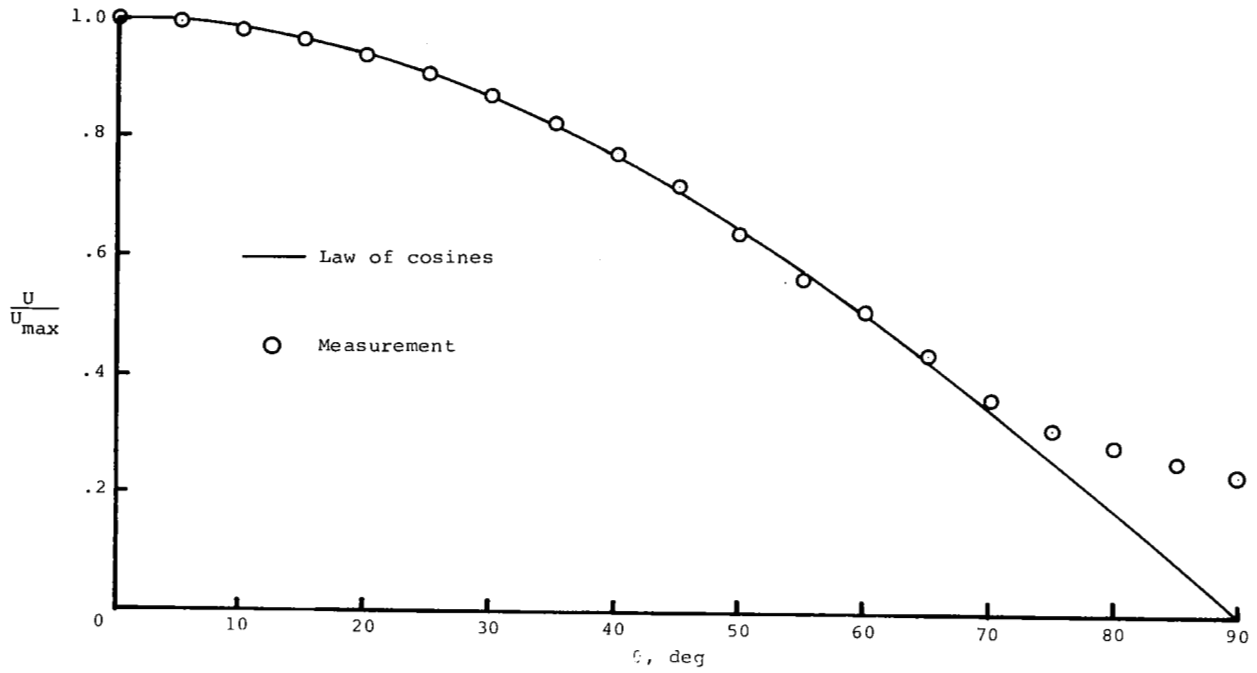

Figure 3.- Typical angular response of one component of x-wire probe.

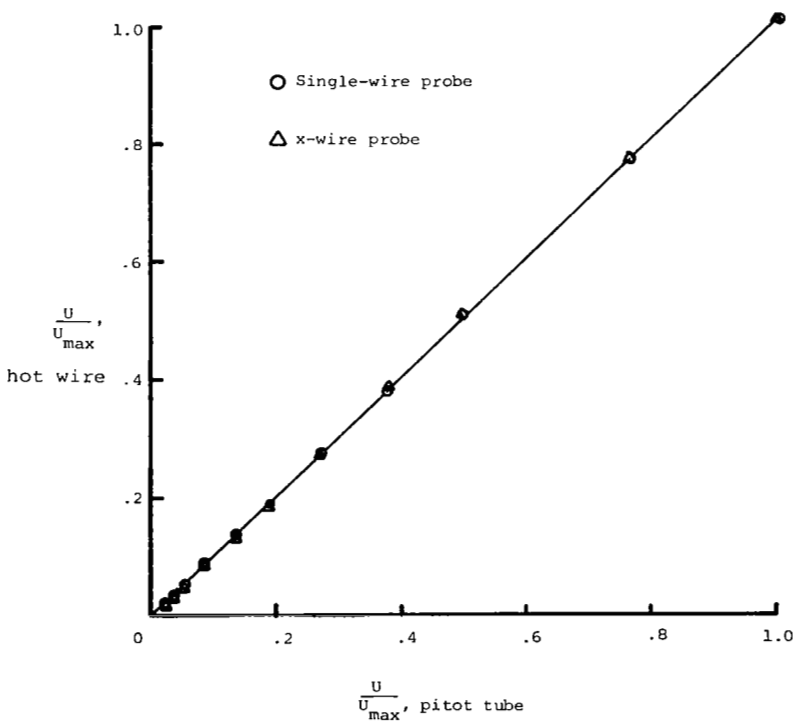

Figure 4.- Hot-wire calibration for mean velocity measurements.

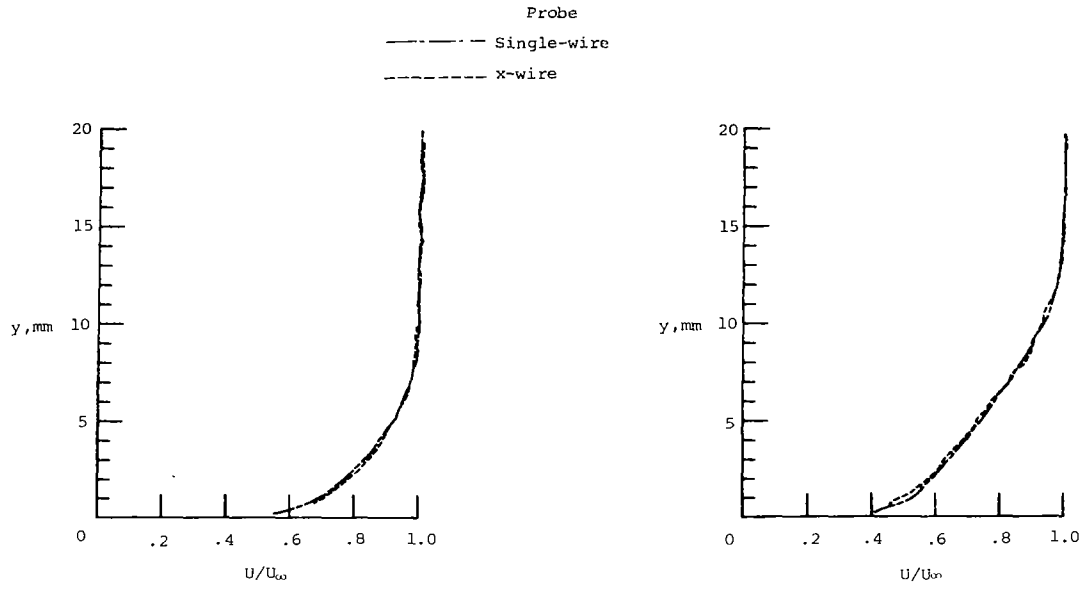

(a) Untripped flow.

(b) Tripped flow.

Figure 5.- Single-wire and x-wire measurements of mean velocity; x/c = 0.9000.

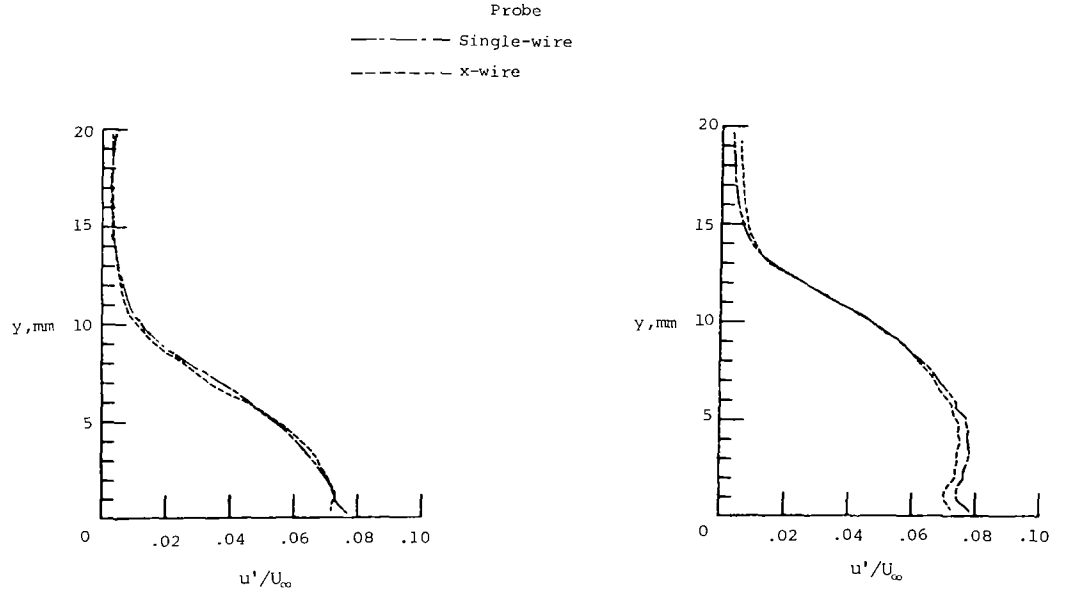

(a) Untripped flow, x/c = 0.9375.

(b) Tripped flow, x/c = 0.9000.

Figure 6.- Single-wire and x-wire measurements of turbulence velocity.

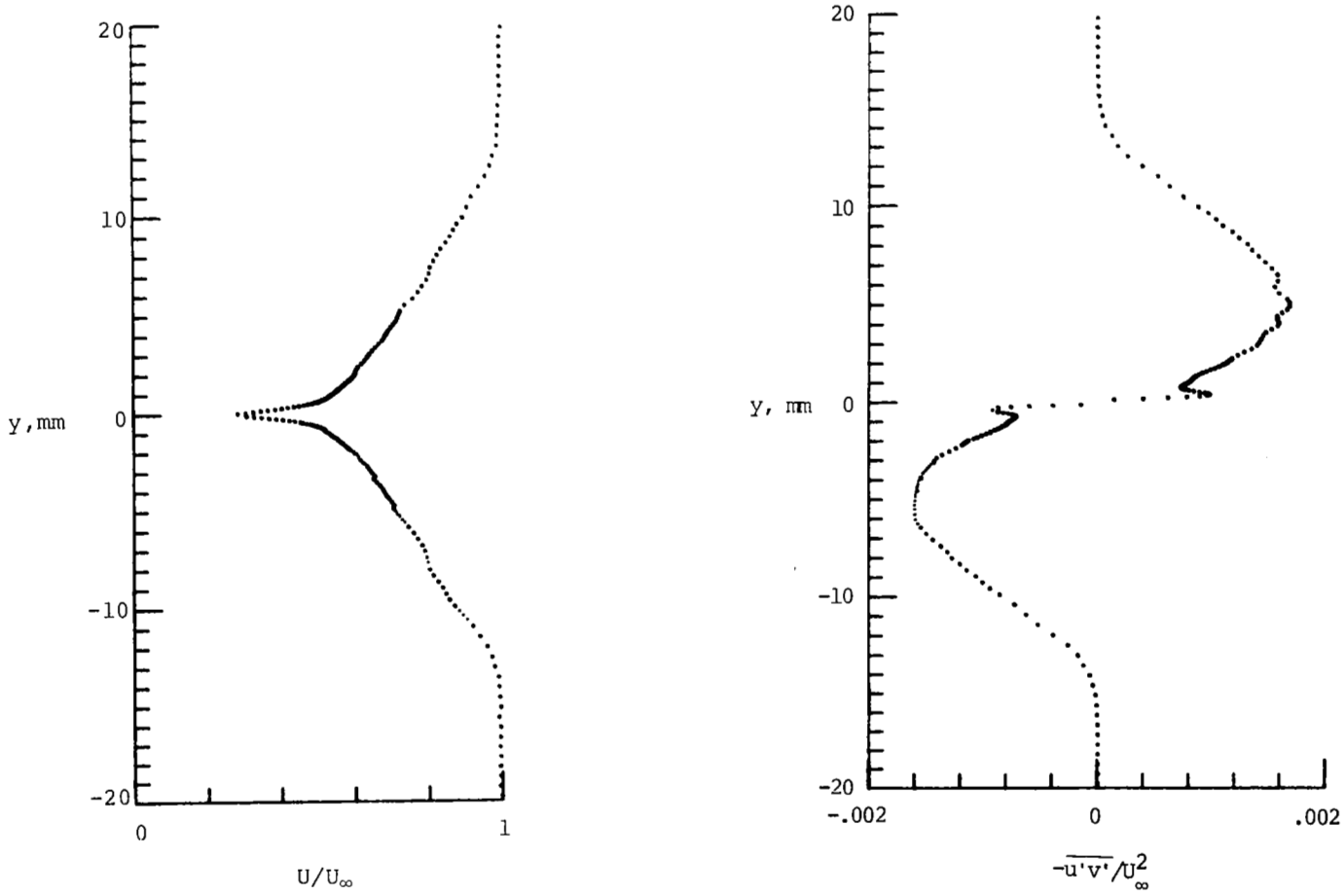

Figure 7.- Distributions of mean velocity and Reynolds shear stress across wake; x/c = 1.0029, tripped flow.

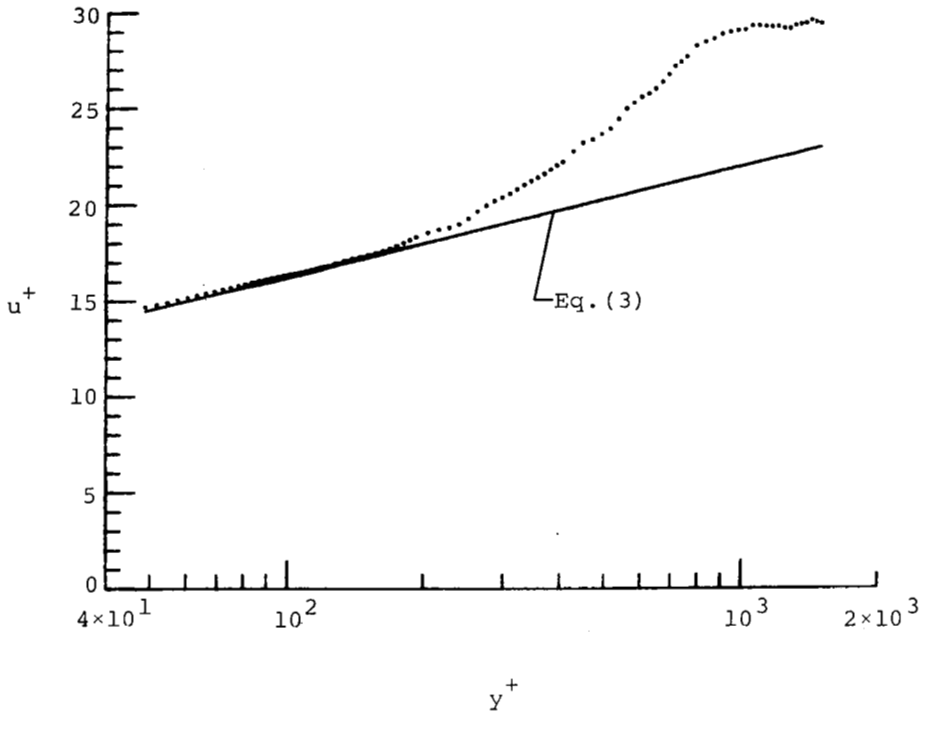

(a) Tripped flow; x/c = 0.9583,

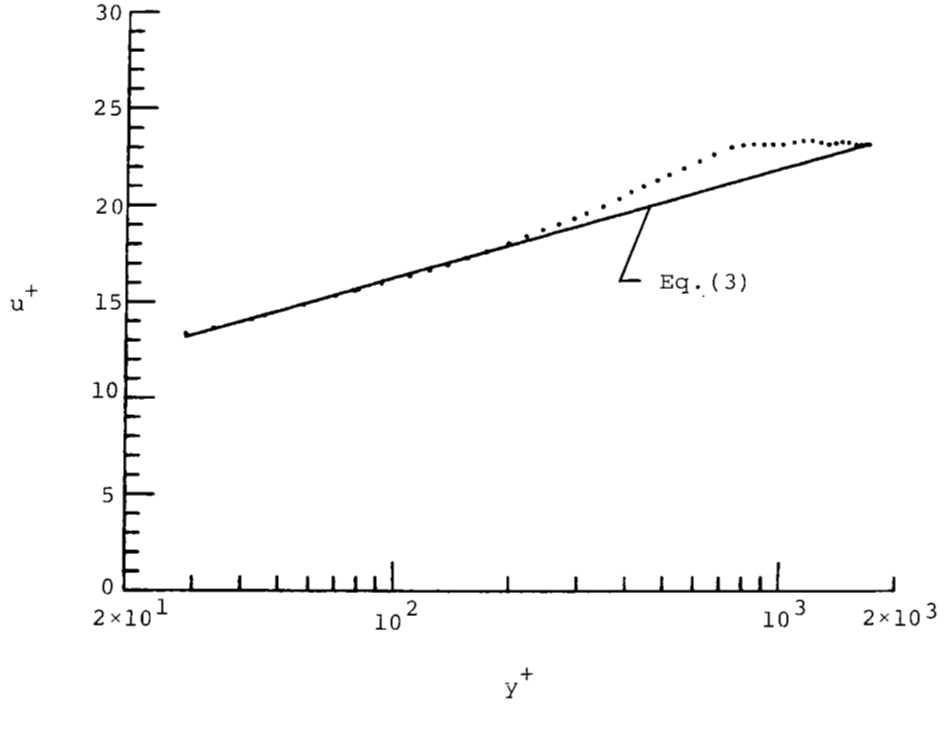

(b) Untripped flow; x/c = 0.9896.

Figure 8.- Comparison between measured velocity and law of wall (eq. (3)).

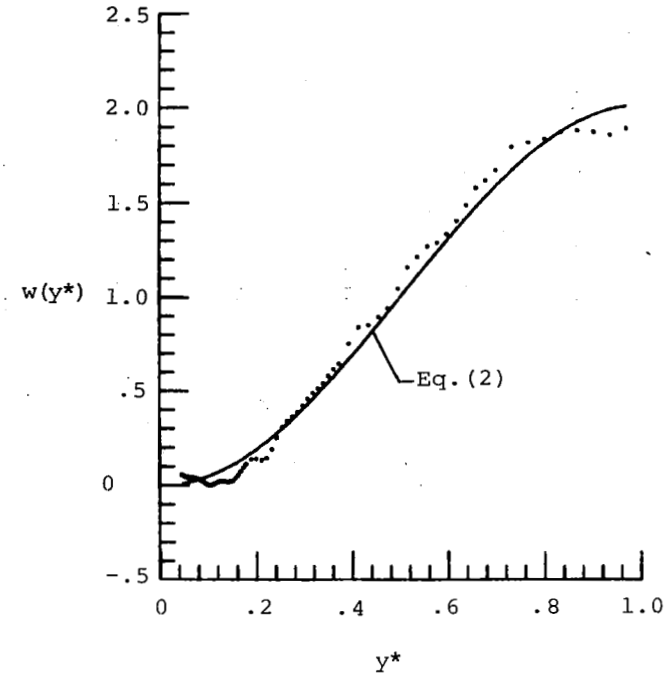

(a) Tripped flow; x/c = 0.9583, α = 1.56.

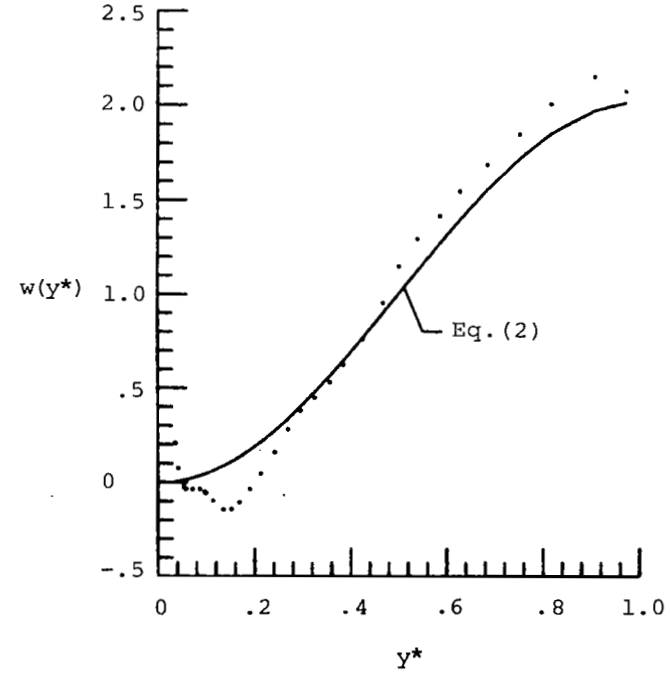

(b) Untripped flow; x/c = 0.9896, α = 0.36.

Figure 9.- Comparison between measured velocity and law of wake (eq. (2)).

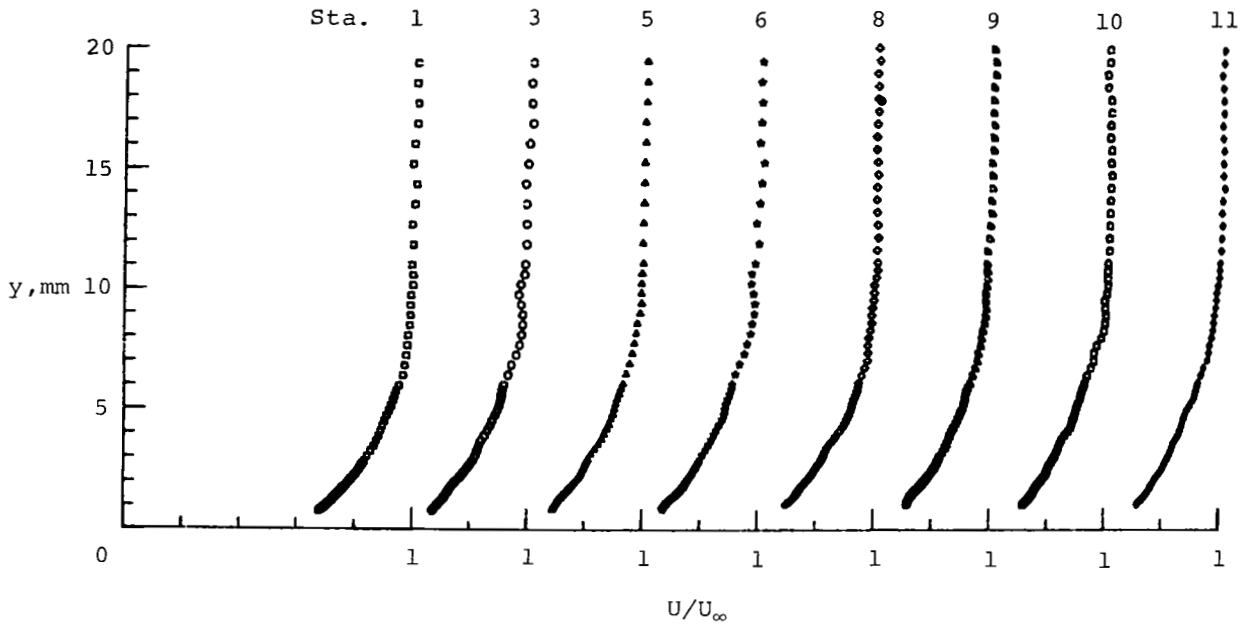

(a) Boundary-layer flow.

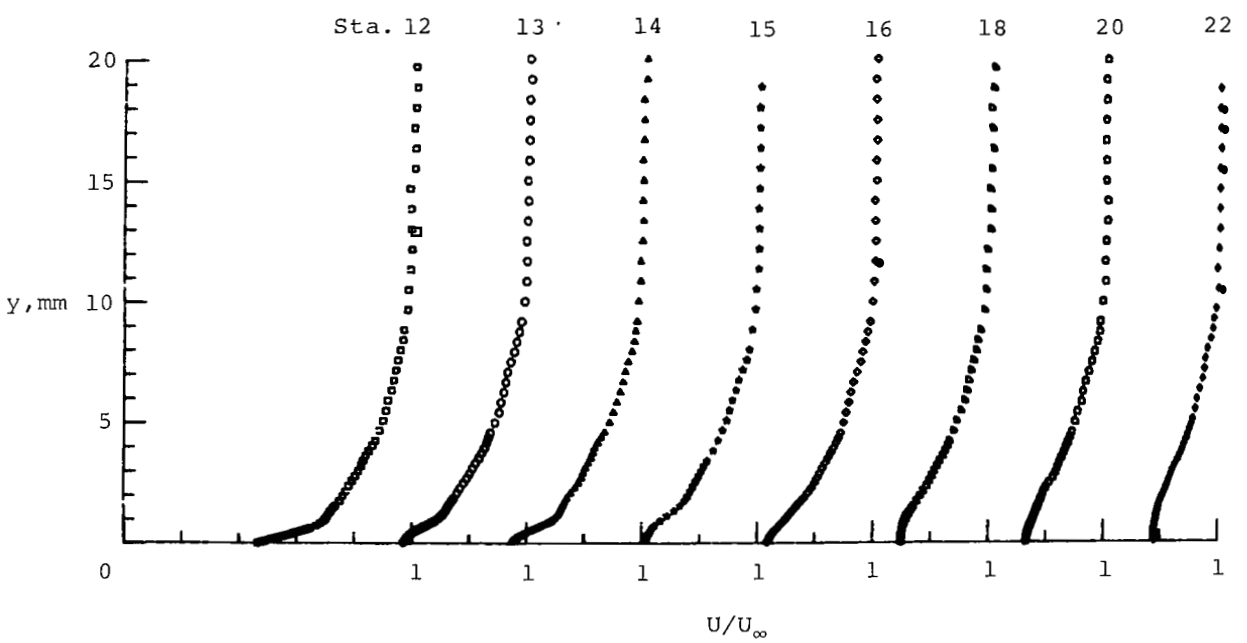

(b) Wake flow.

Figure 10.- Mean velocity distribution; untripped.

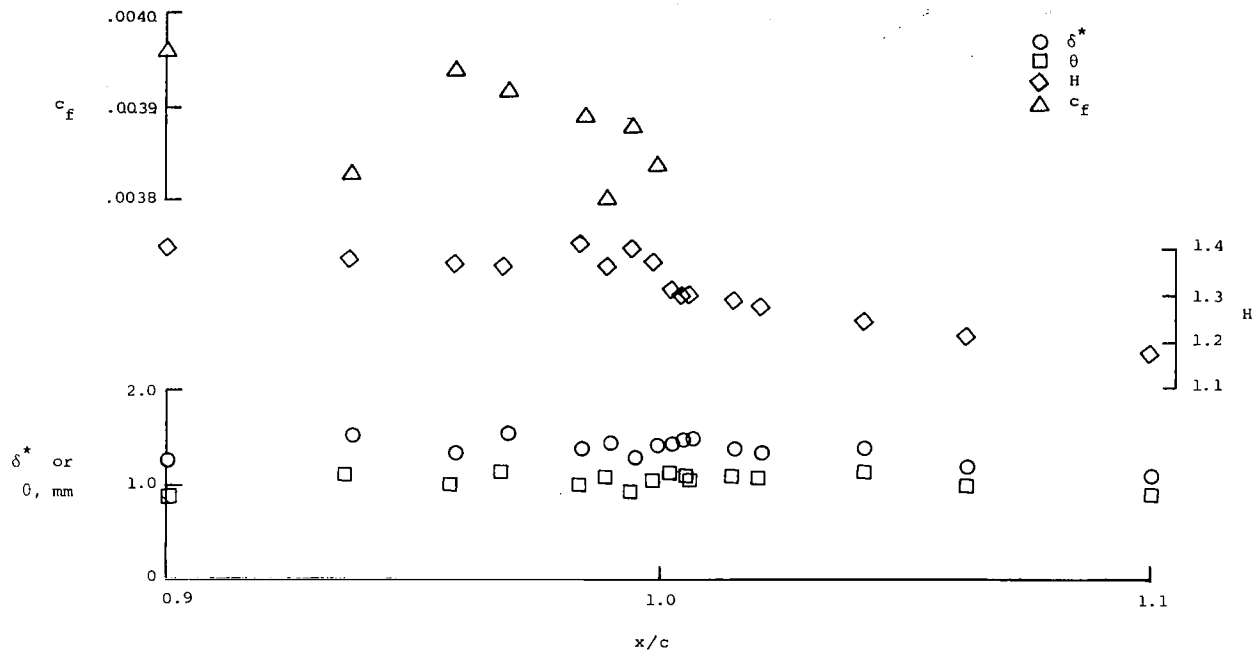

Figure 11.- Distribution of mean-flow integral properties; untripped flow.

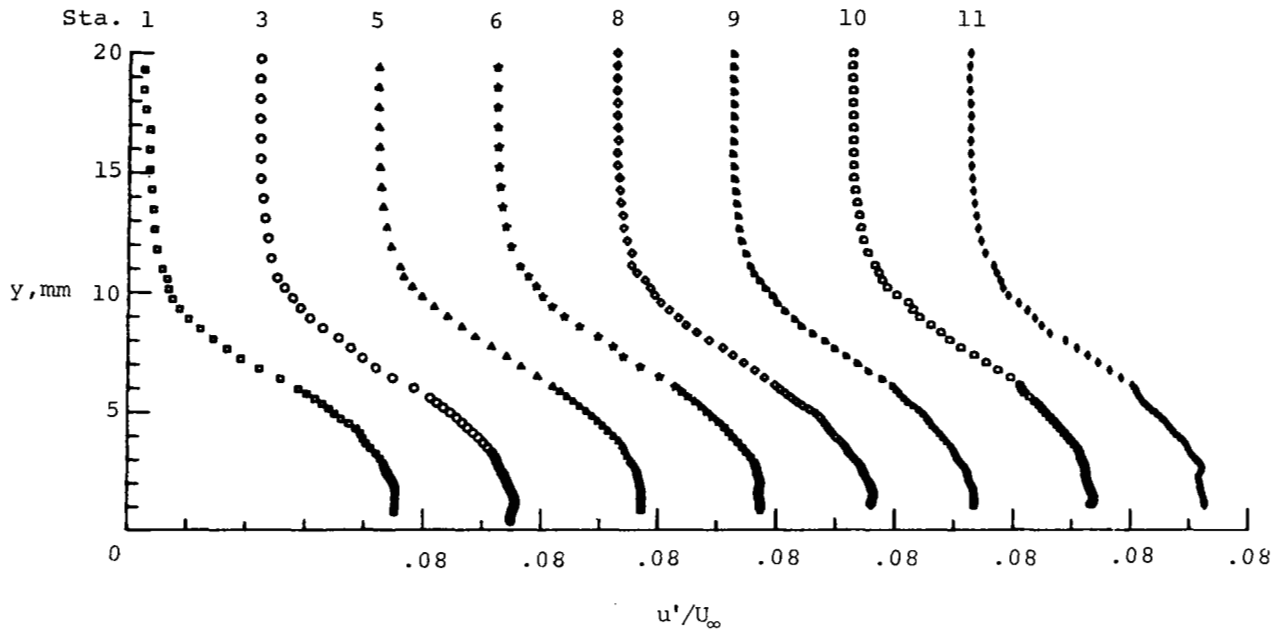

(a) Boundary-layer flow.

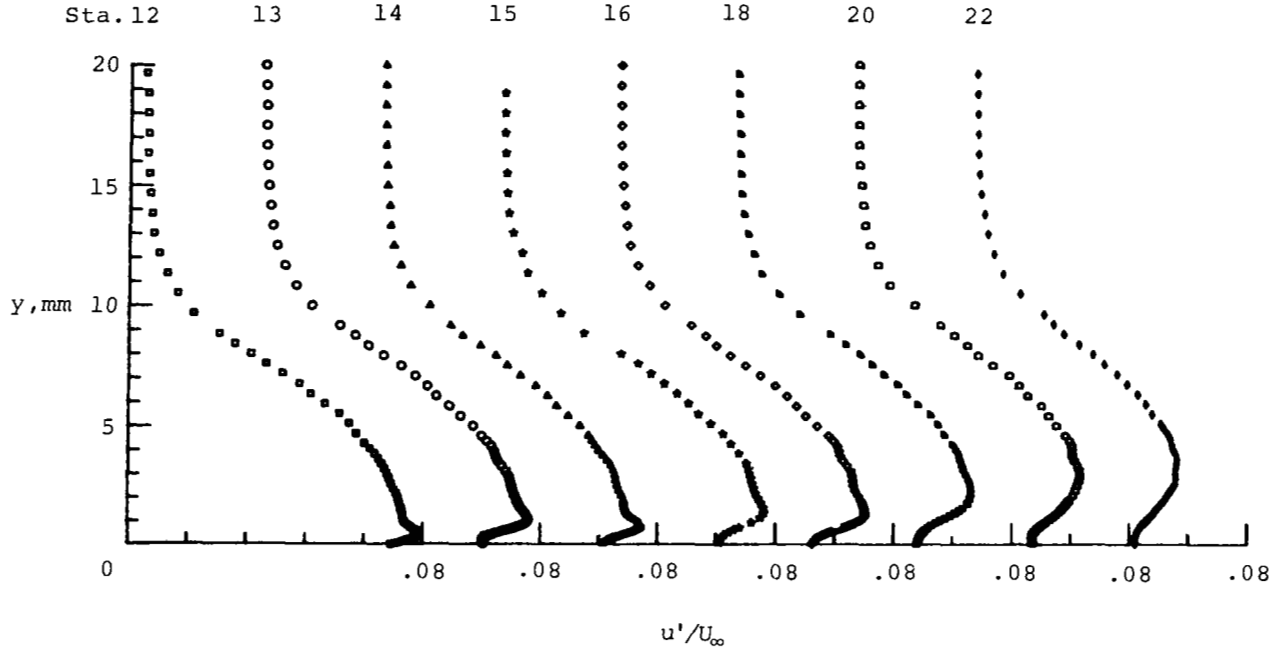

(b) Wake flow.

Figure 12.- Distribution of streamwise turbulent intensity; untripped.

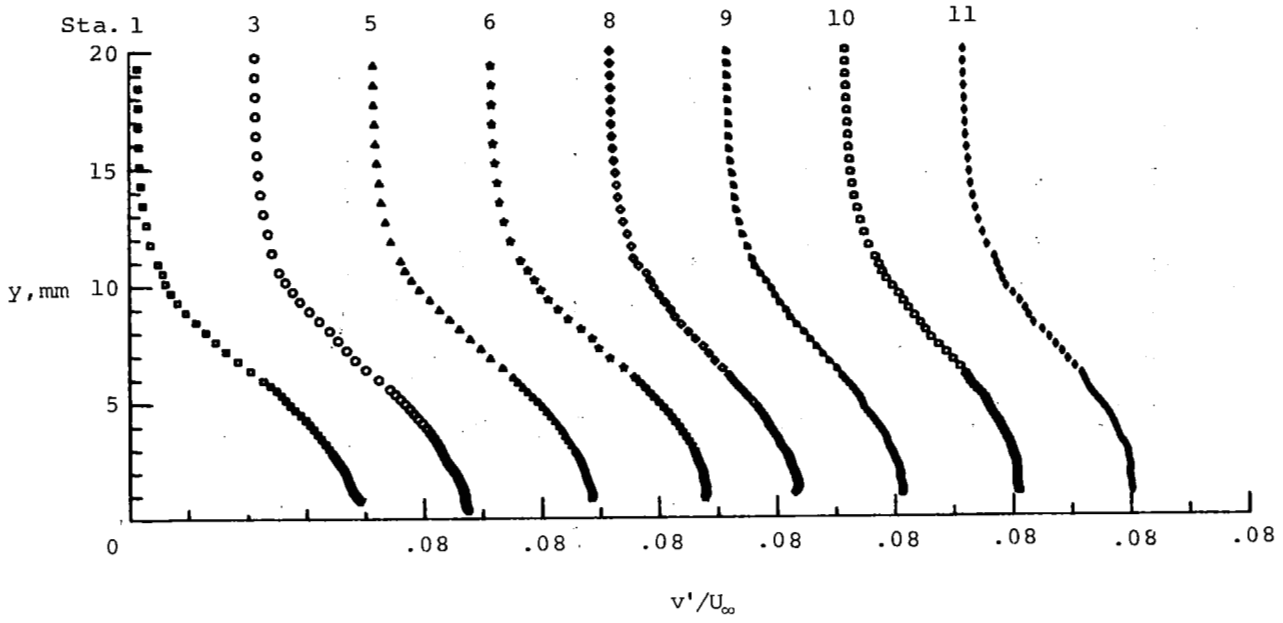

(a) Boundary-layer flow.

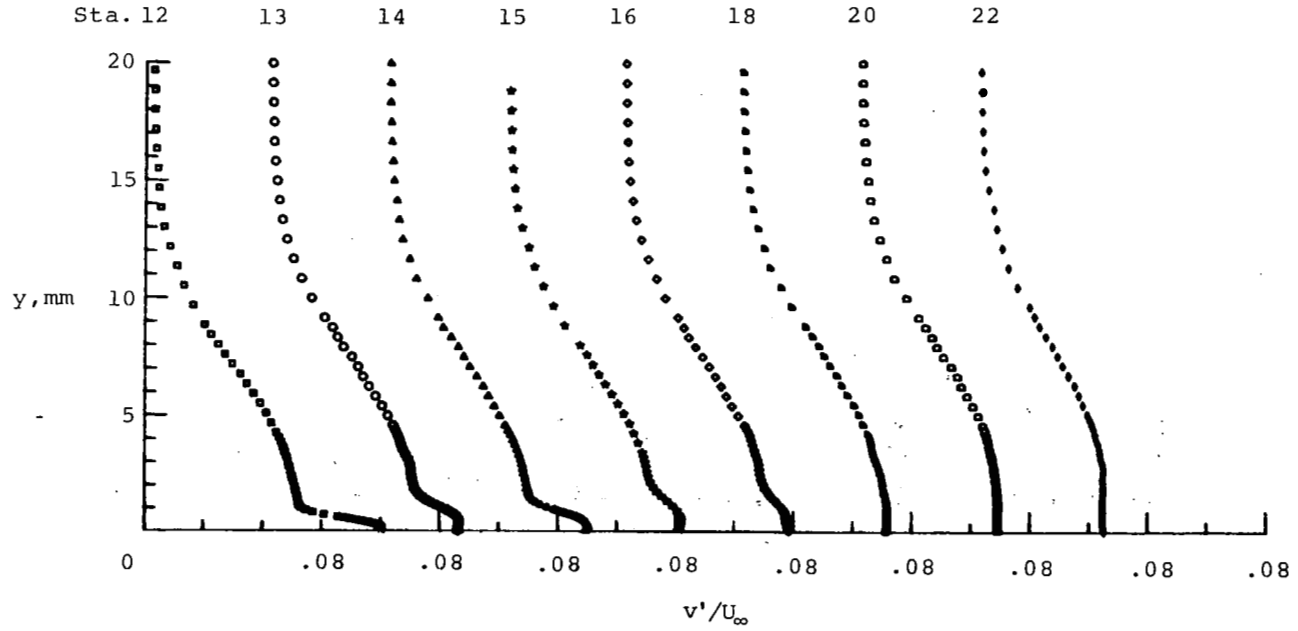

(b) Wake flow.

Figure 13.- Distribution of transverse turbulent intensity; untripped.

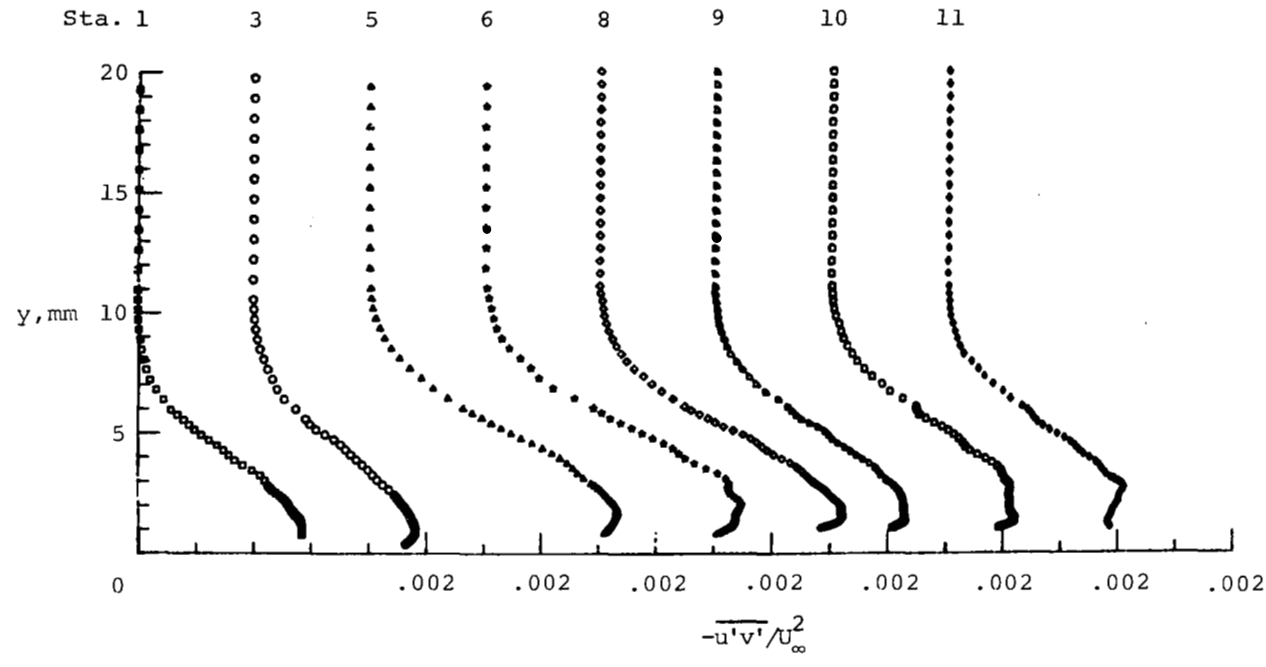

(a) Boundary-layer flow.

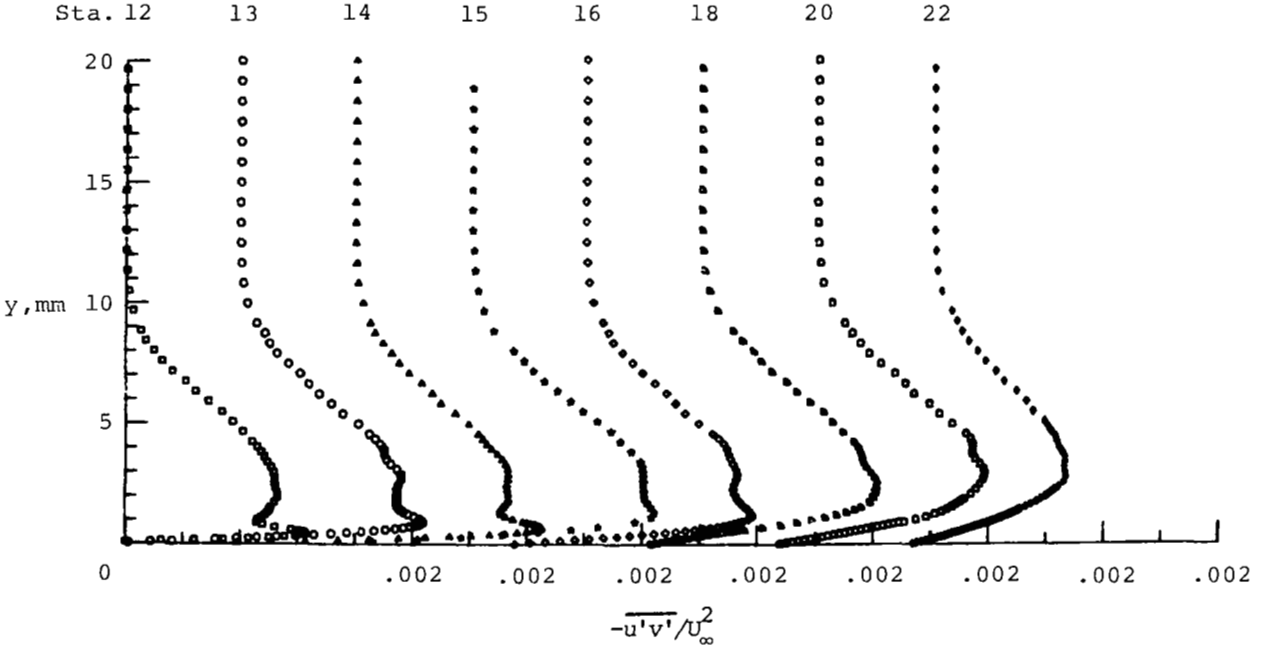

(b) Wake flow.

Figure 14.- Distribution of Reynolds shear stress; untripped.

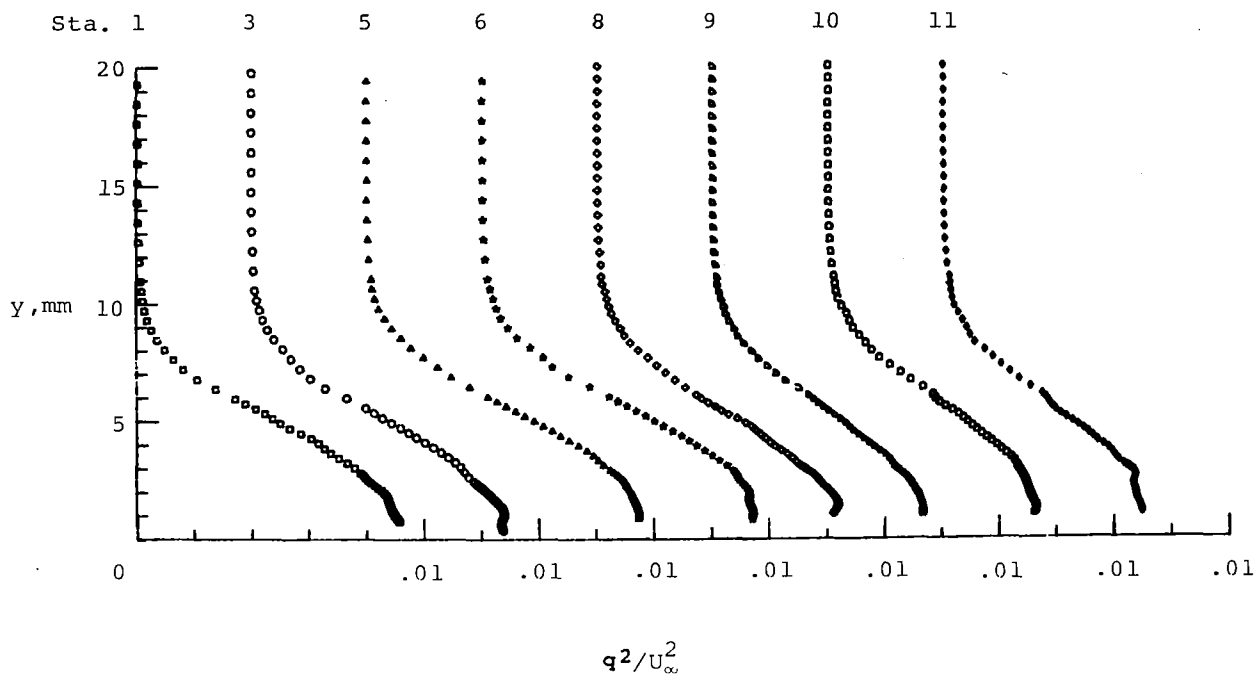

(a) Boundary-layer flow.

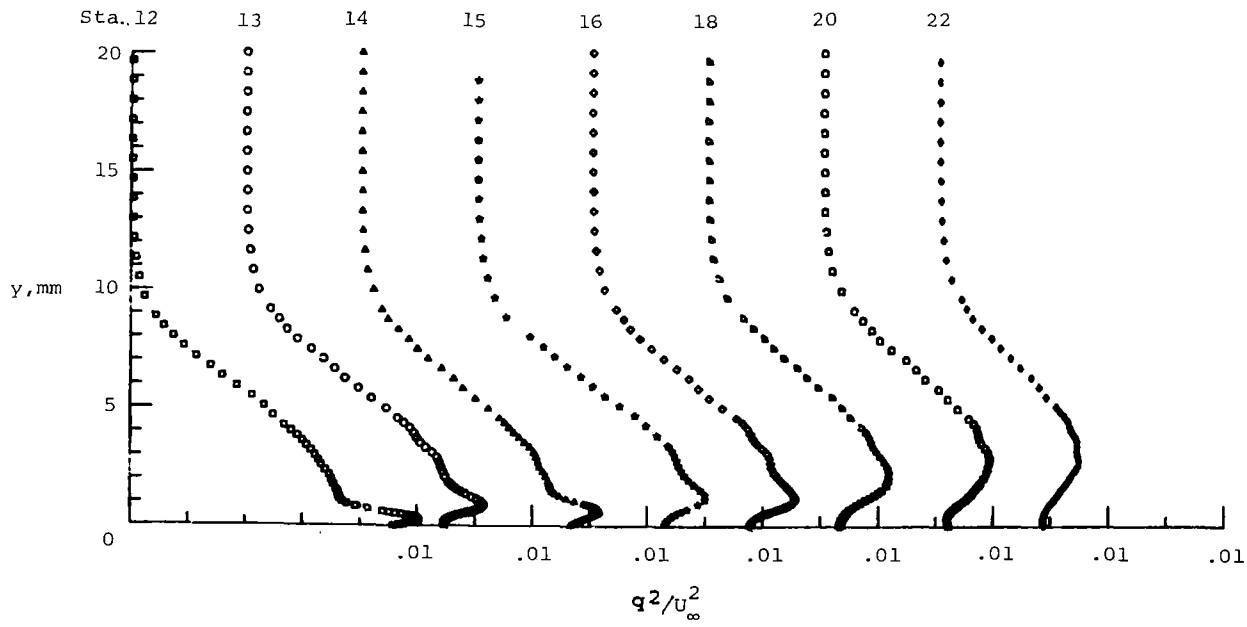

(b) Wake flow.

Figure 15.- Distribution of turbulent-kinetic-energy flux; untripped.

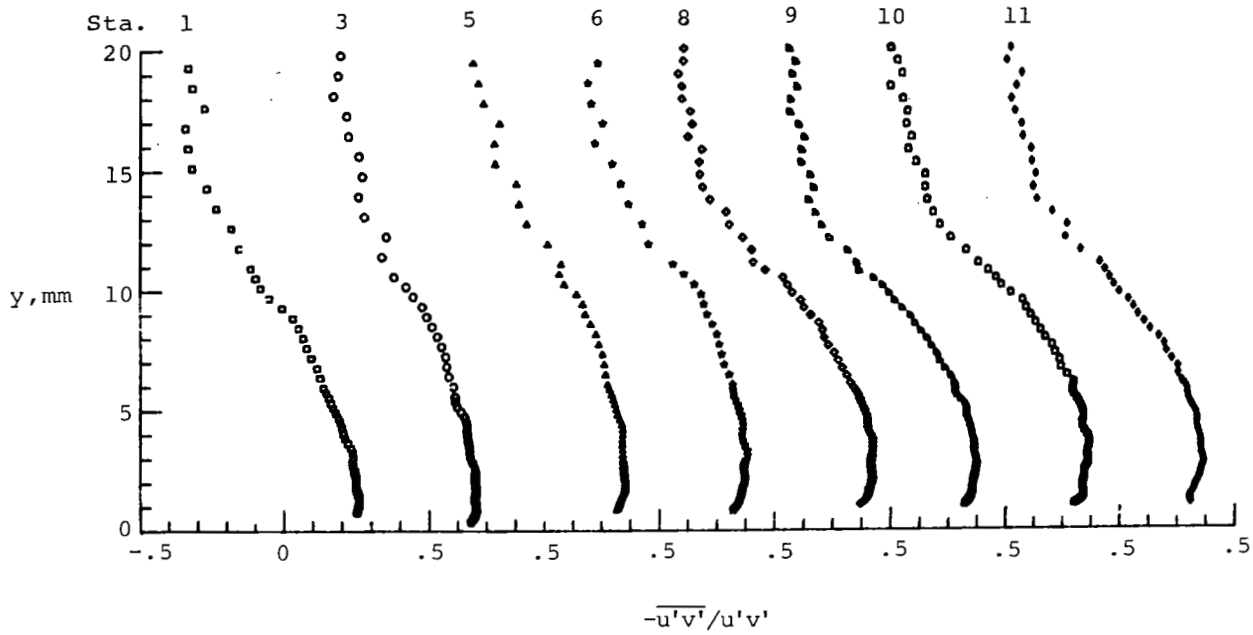

(a) Boundary-layer flow.

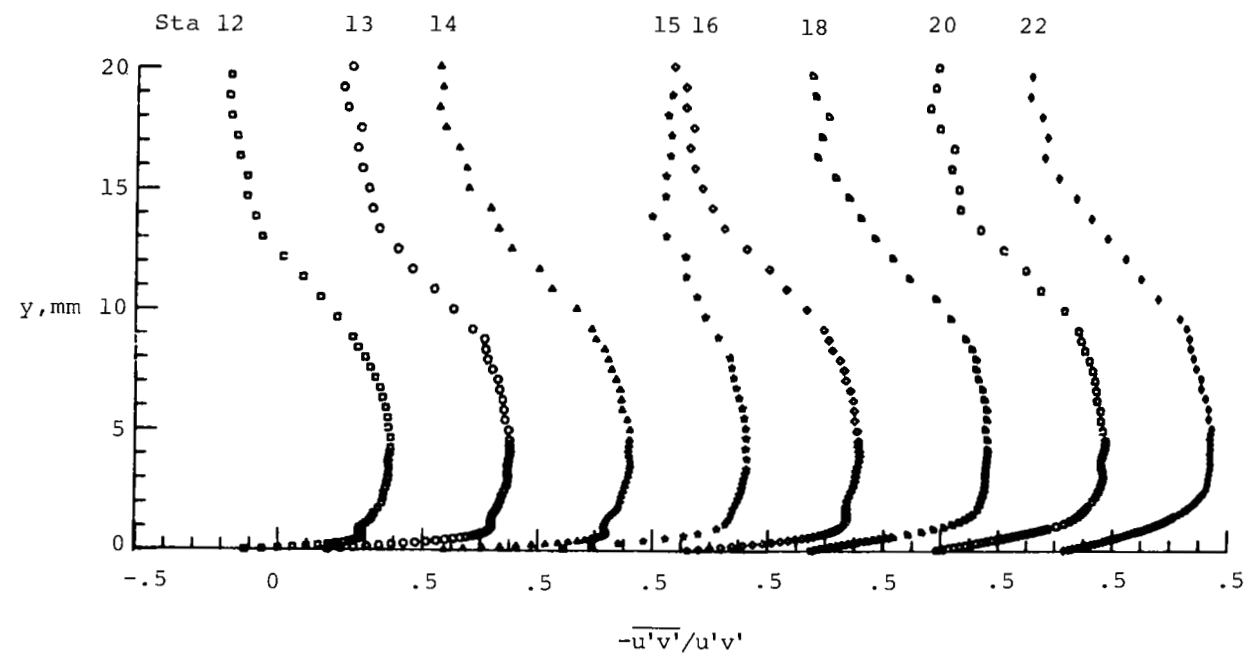

(b) Wake flow.

Figure 16.- Distribution of turbulent-shear correlation coefficient; untripped.

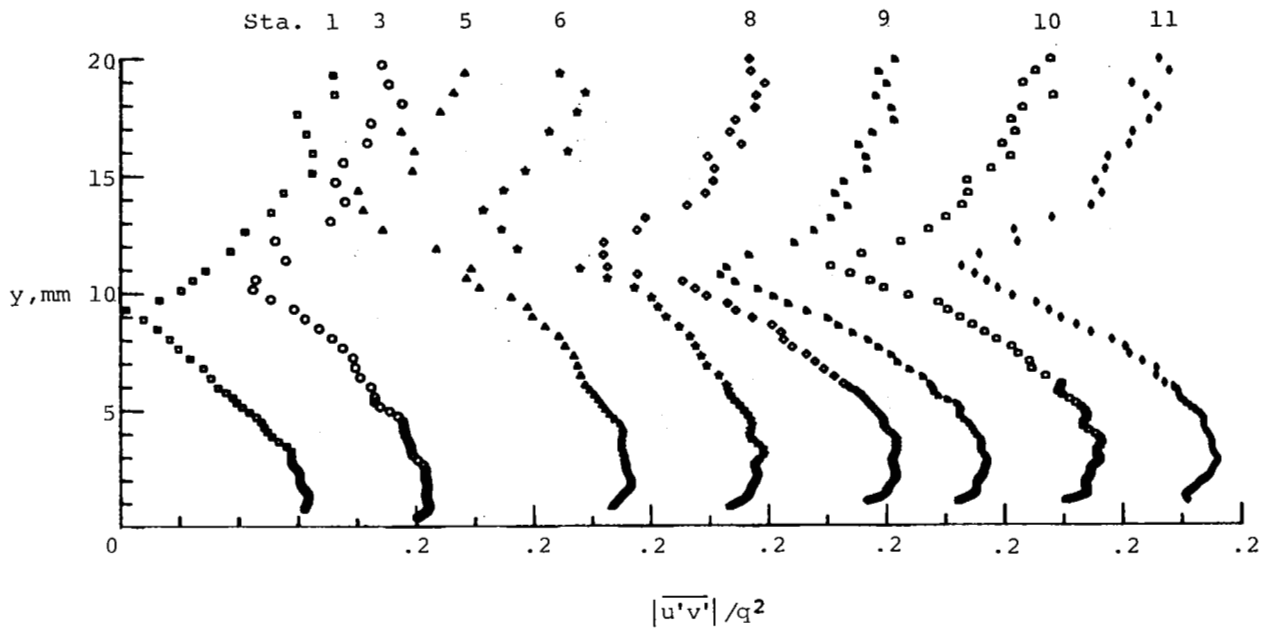

(a) Boundary-layer flow.

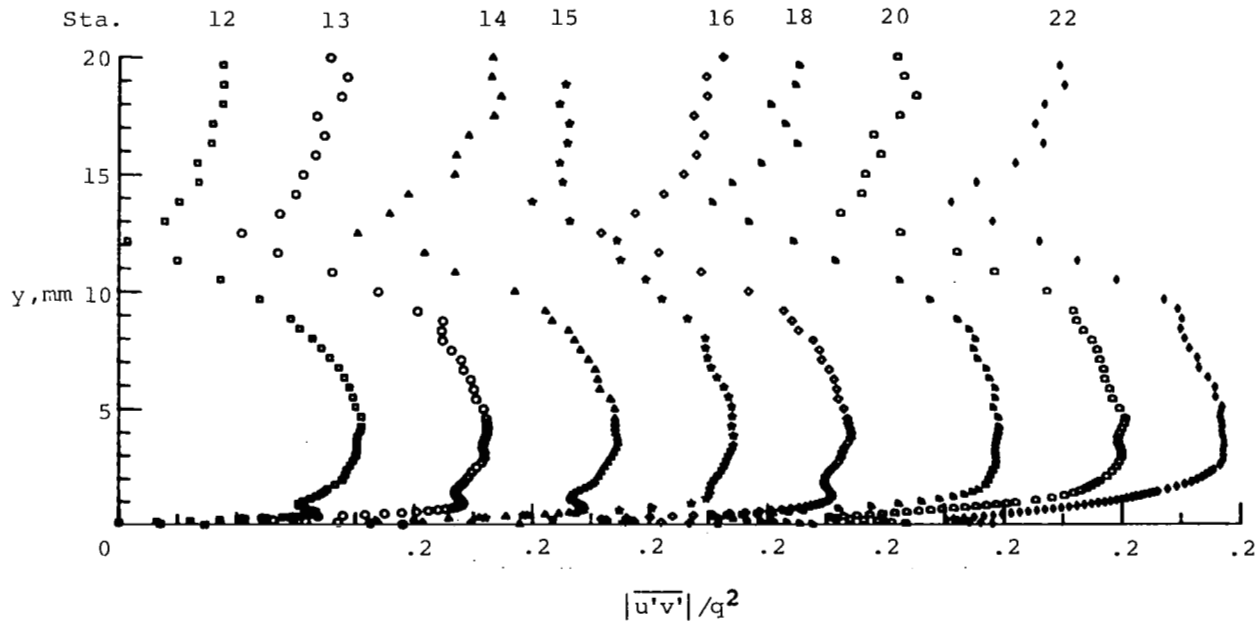

(b) Wake flow.

Figure 17.- Distribution of ratio of Reynolds shear stress and turbulent kinetic energy; untripped.

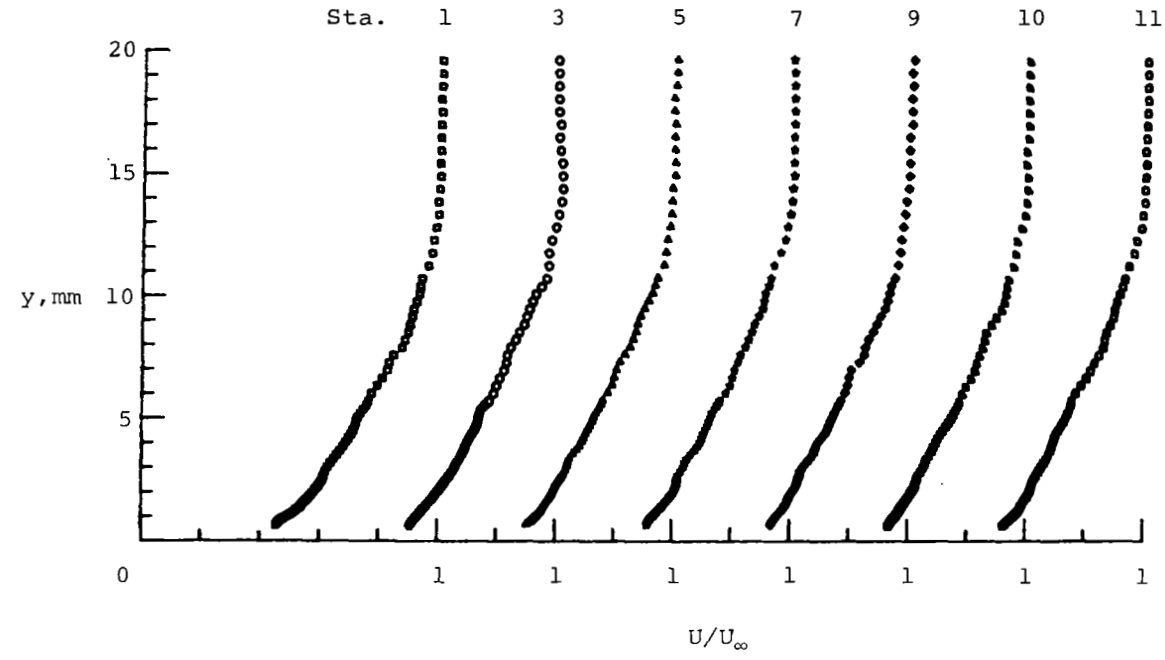

(a) Boundary-layer flow.

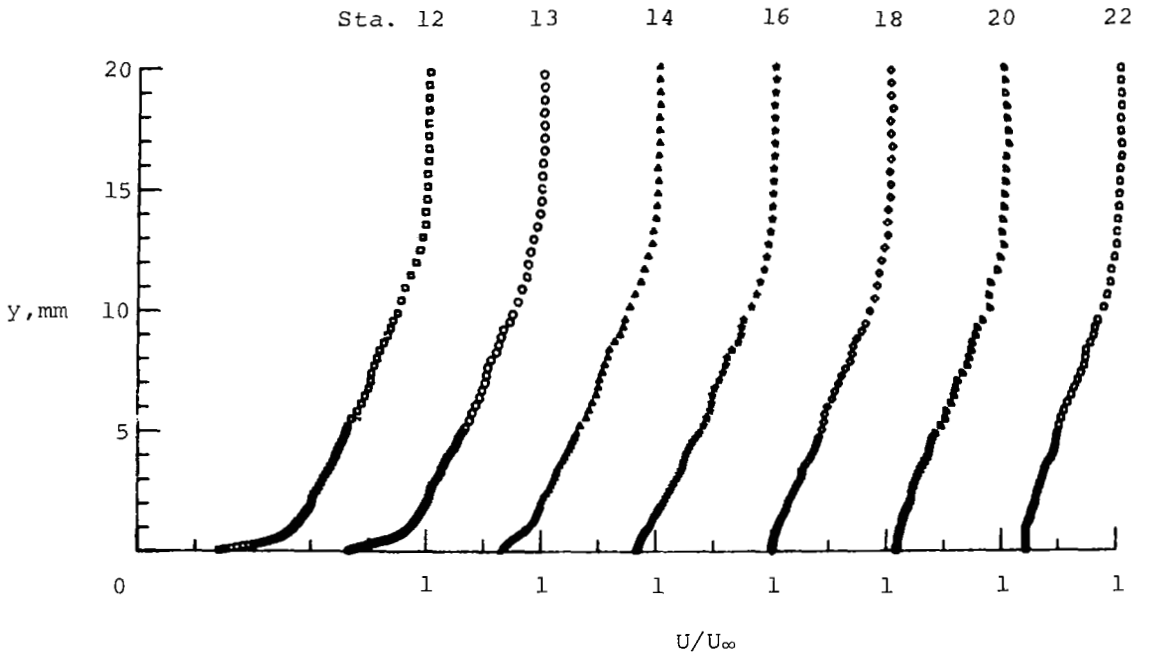

(b) Wake flow.

Figure 18.- Mean velocity distribution; tripped.

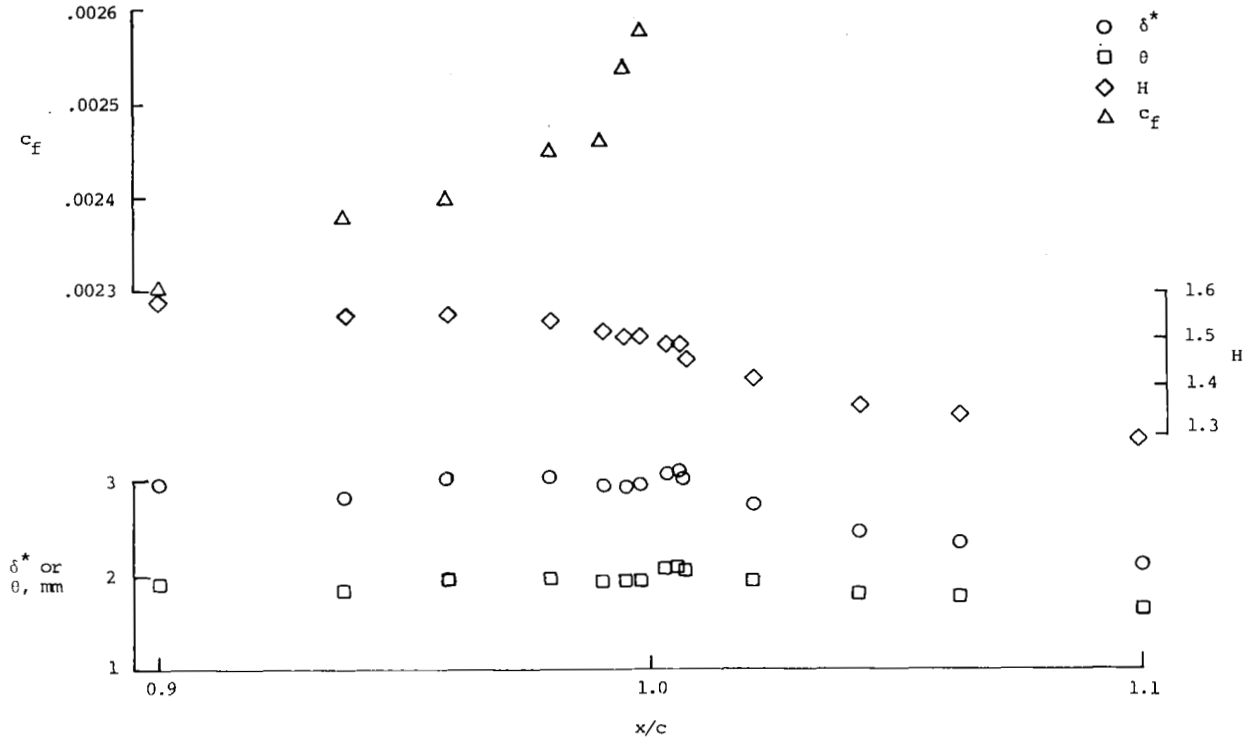

Figure 19.- Distribution of mean-flow integral properties; tripped flow.

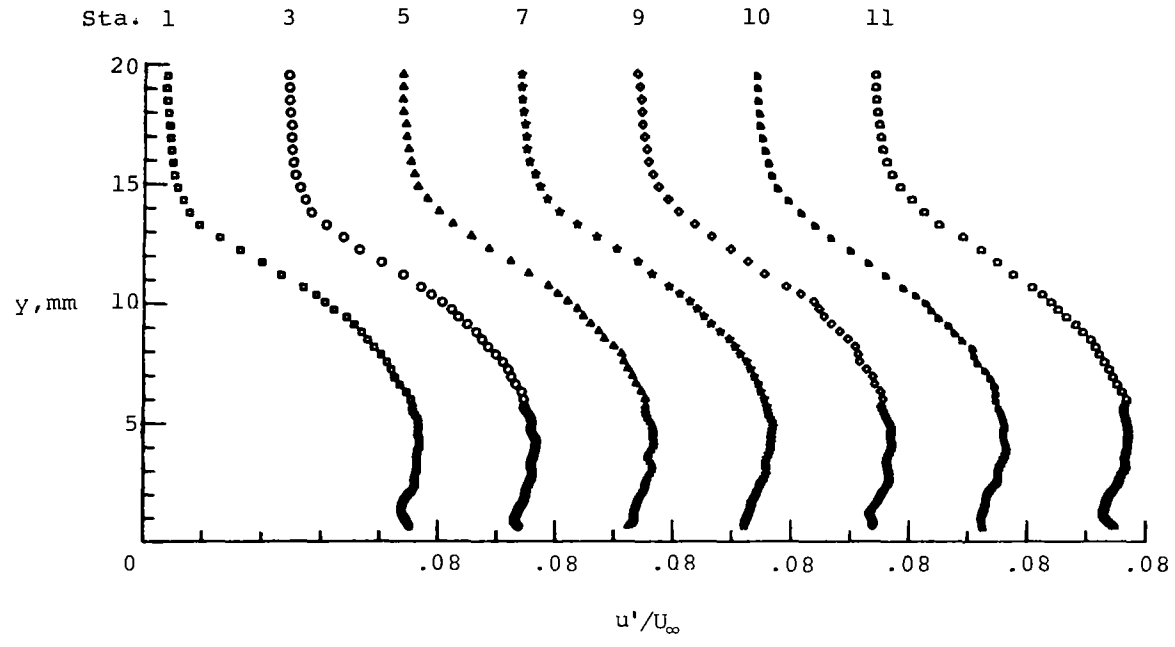

(a) Boundary-layer flow.

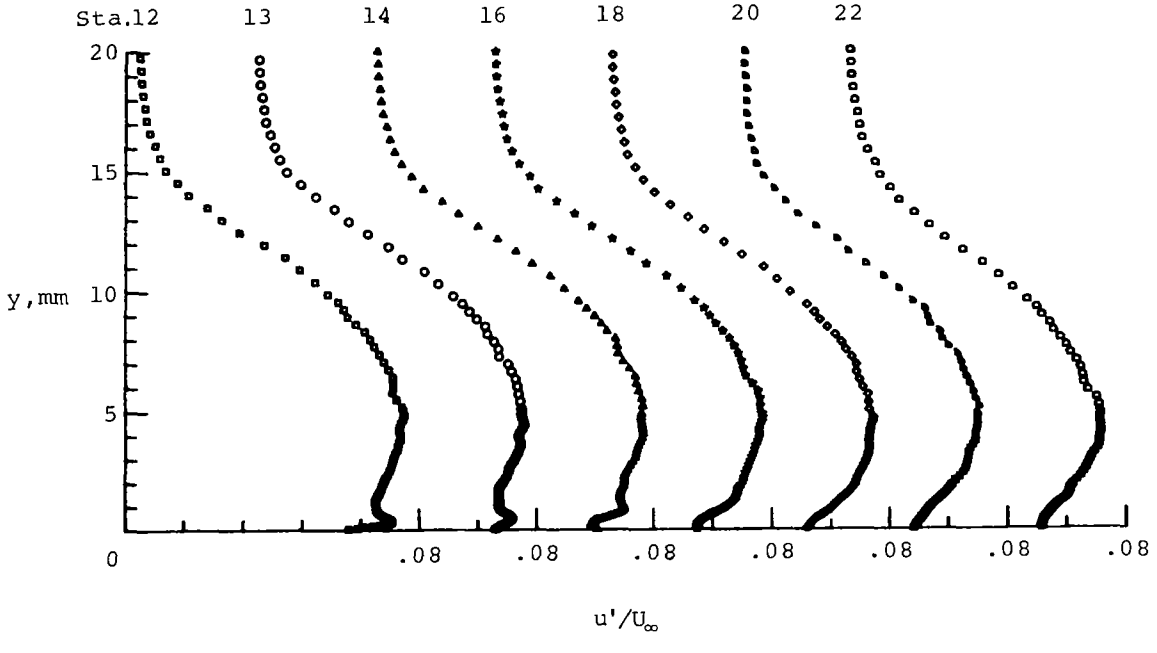

(b) Wake flow.

Figure 20.- Distribution of streamwise turbulent intensity; tripped flow.

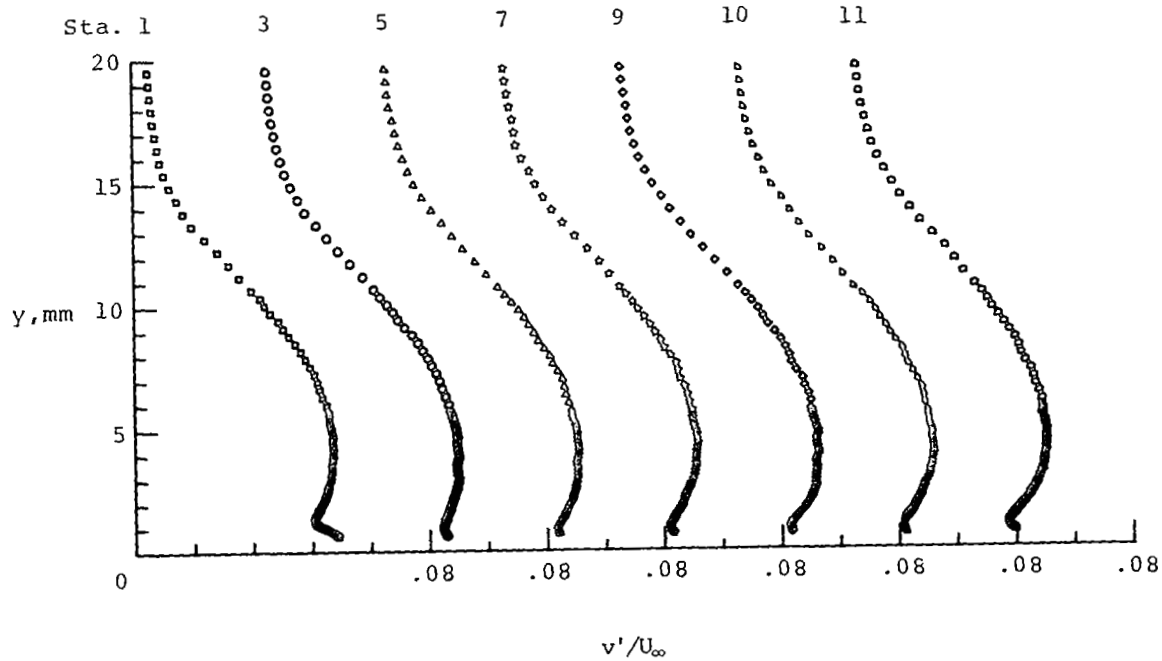

(a) Boundary-layer flow.

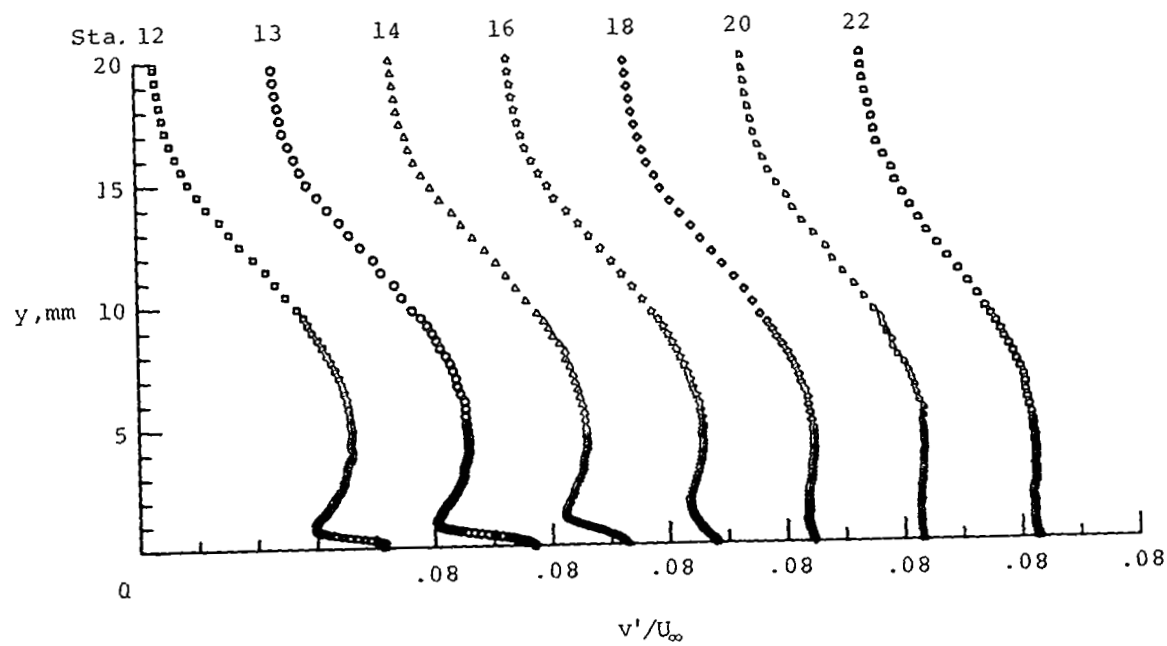

(b) Wake flow.

Figure 21.- Distribution of transverse turbulent intensity; tripped.

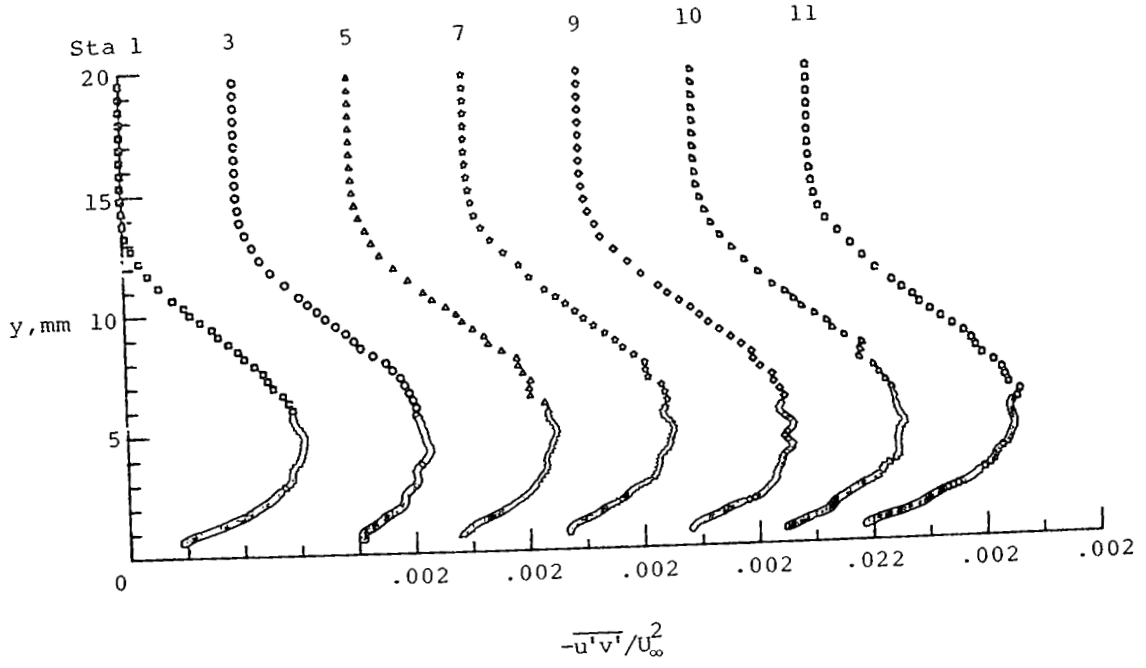

(a) Boundary-layer flow.

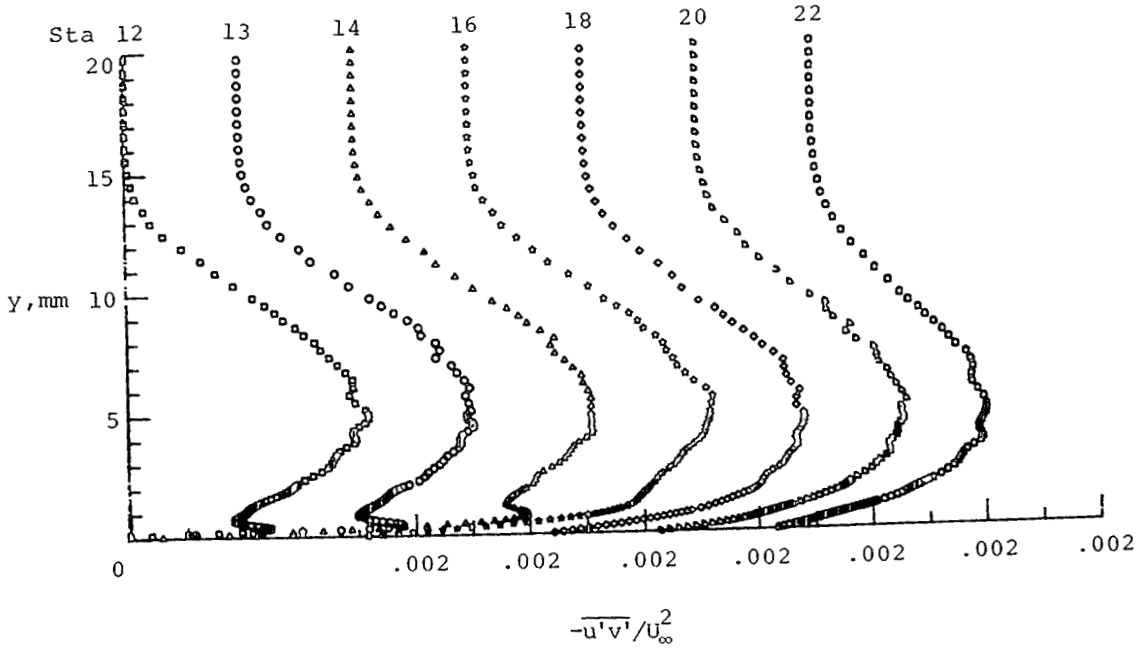

(b) Wake flow.

Figure 22.- Distribution of Reynolds shear stress; tripped.

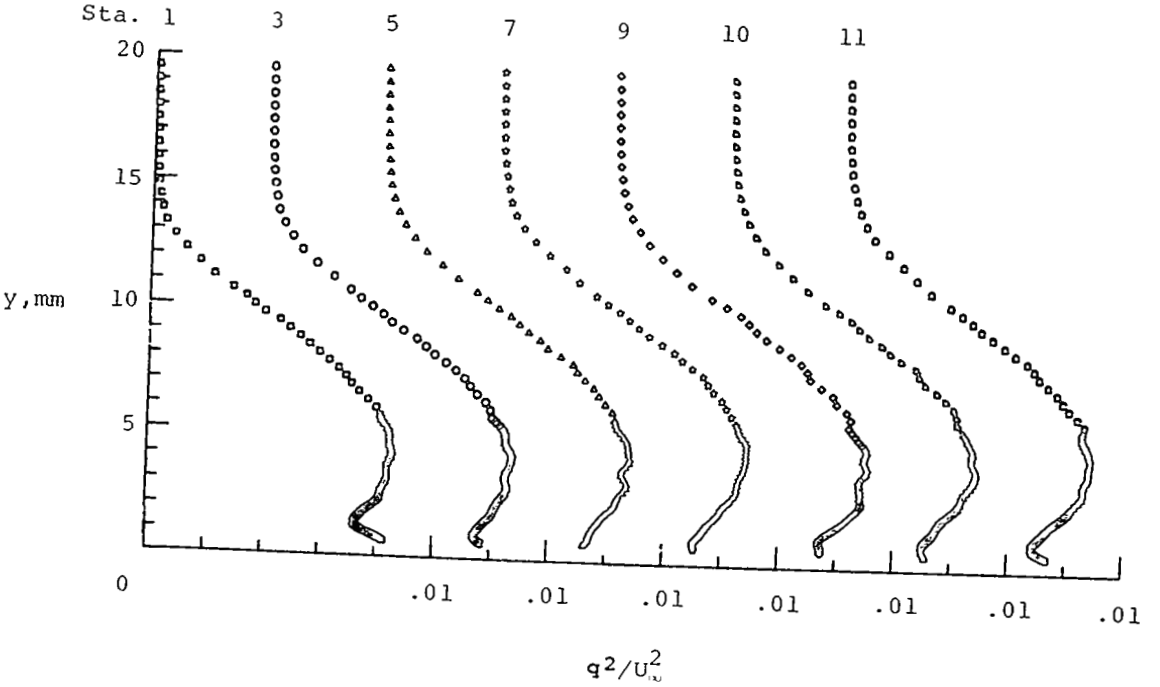

(a) Boundary-layer flow.

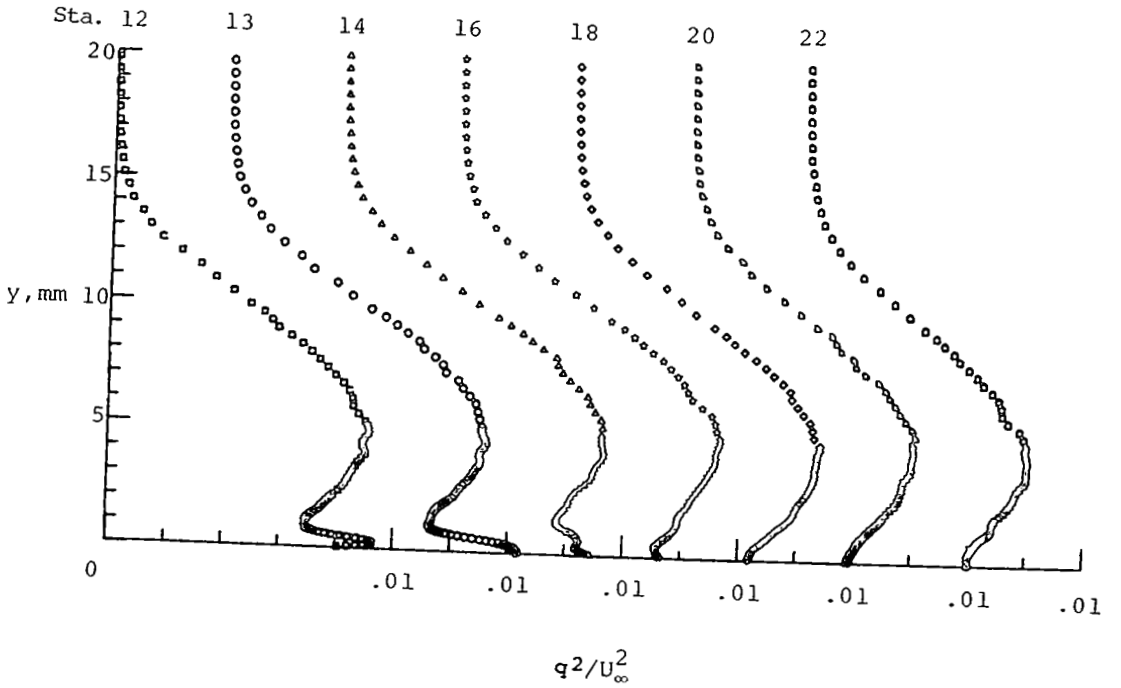

(b) Wake flow.

Figure 23.- Distribution of turbulent kinetic energy; tripped.

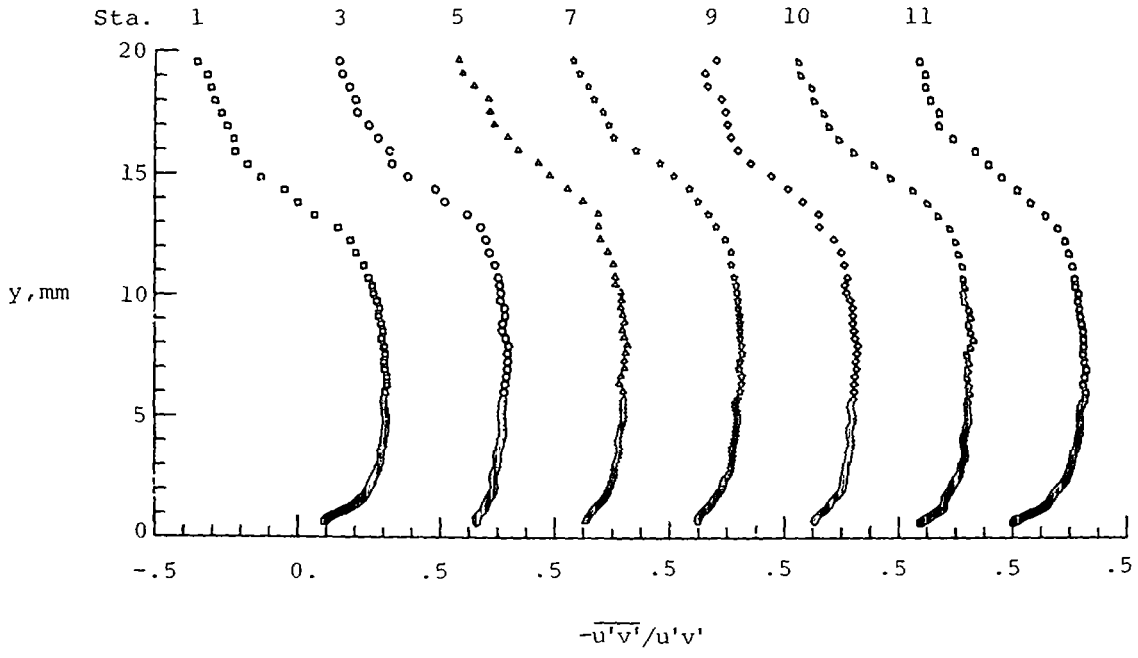

(a) Boundary-layer flow.

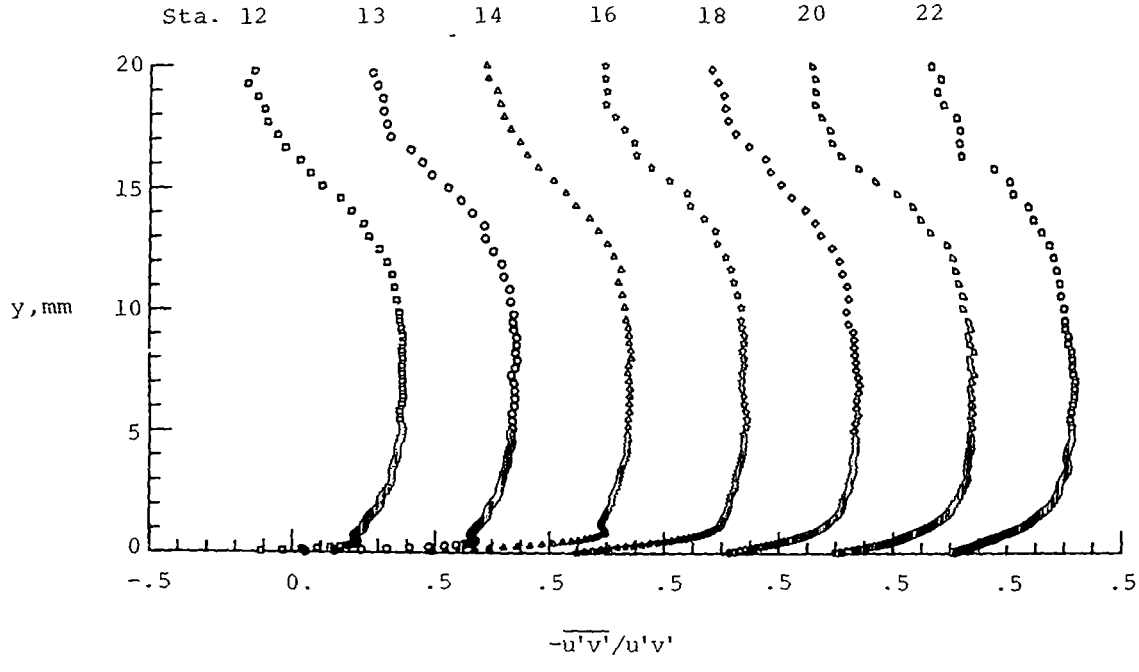

(b) Wake flow.

Figure 24.- Distribution of turbulent-shear correlation coefficient; tripped.

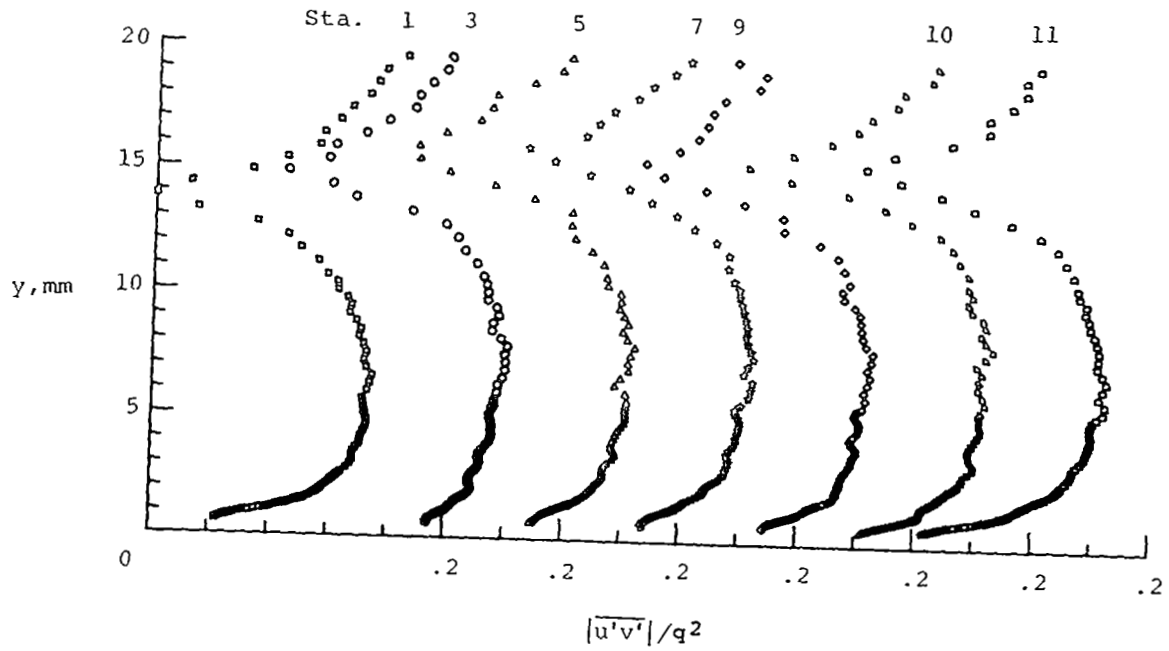

(a) Boundary-layer flow.

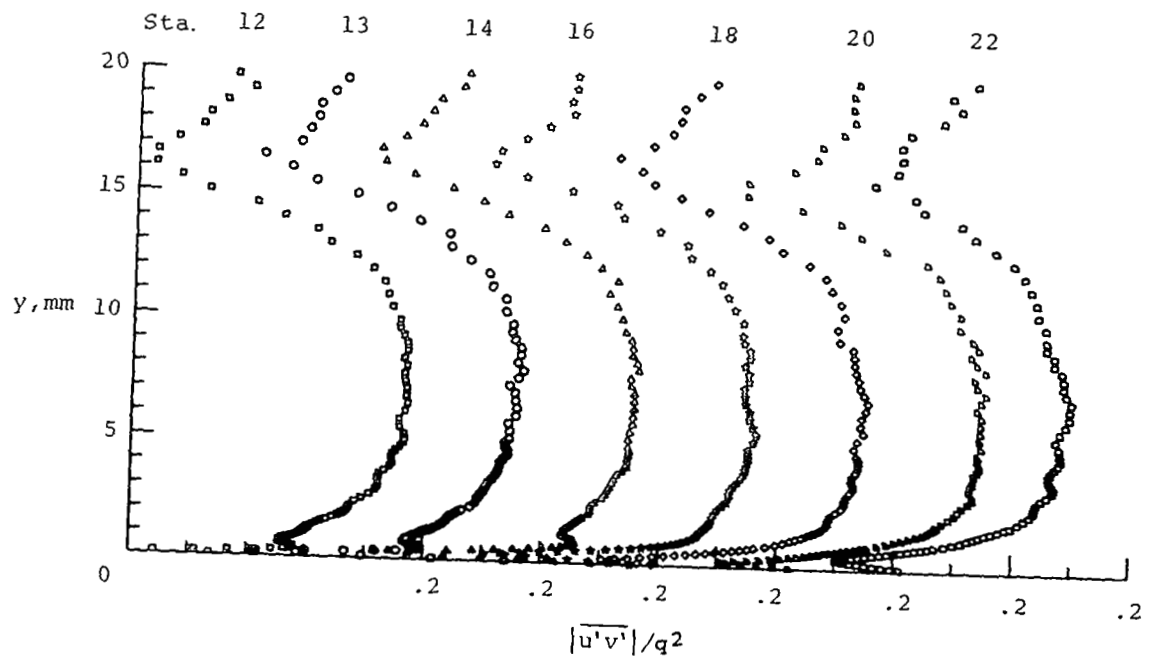

(b) Wake flow.

Figure 25.- Distribution of ratio of Reynolds shear stress and turbulent kinetic energy; tripped.

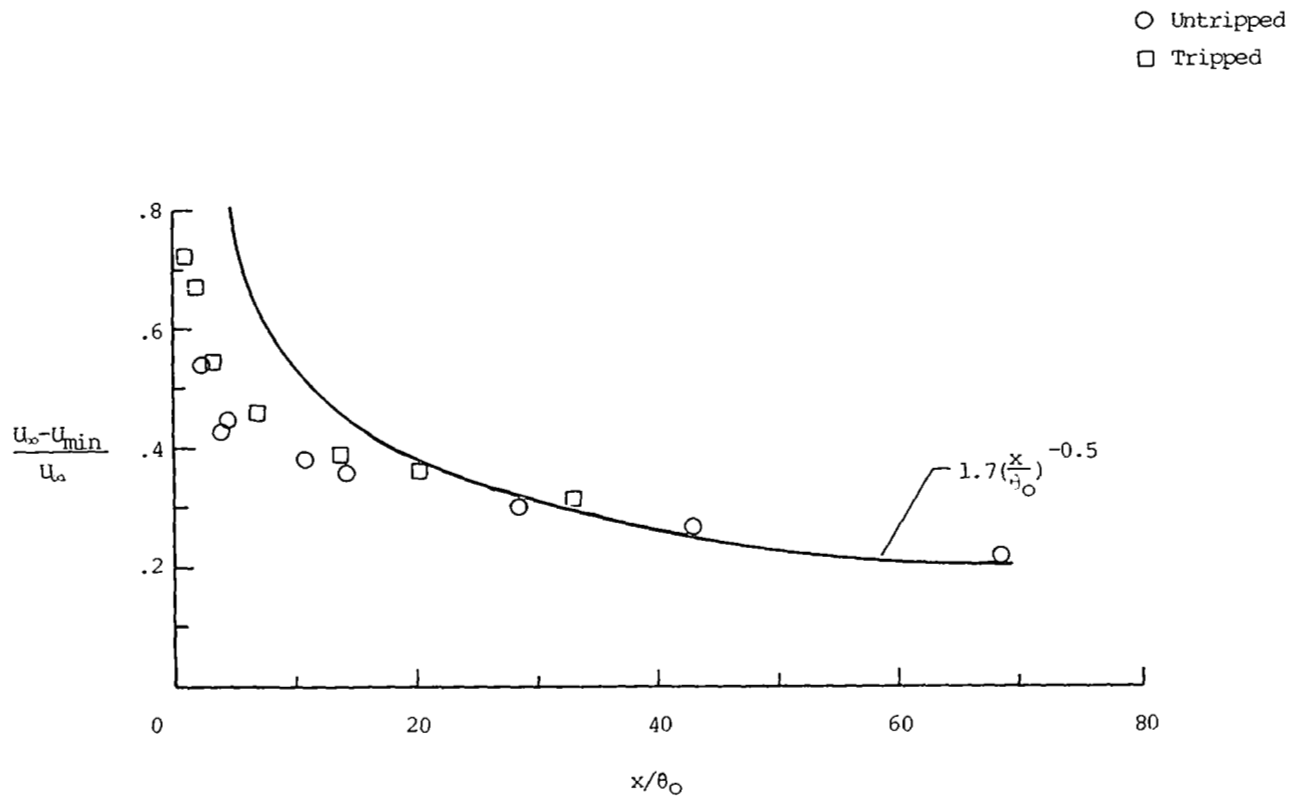

Figure 26.- Similarity of wake-velocity defect distribution.

1. Report No.	2. Government Accession No.	3. Recipient's Catalog No.
NASA TP-1845		

4. Title and Subtitle	5. Report Date
MEAN-FLOW AND TURBULENCE MEASUREMENTS IN THE VICINITY OF THE TRAILING EDGE OF AN NACA 63_1-012 AIRFOIL	May 1981
	6. Performing Organization Code 505-32-03-05

7. Author(s)	8. Performing Organization Report No.
James C. Yu	L-13959
	10. Work Unit No.

9. Performing Organization Name and Address	11. Contract or Grant No.
NASA Langley Research Center Hampton, VA 23665	
	13. Type of Report and Period Covered Technical Paper

12. Sponsoring Agency Name and Address	14. Sponsoring Agency Code
National Aeronautics and Space Administration Washington, DC 20546	

15. Supplementary Notes

16. Abstract

Mean-flow and turbulence measurements have been conducted in the vicinity of a cusped-trailing edge of a two-dimensional NACA 63_1-012 airfoil at zero angle of attack. Naturally transitioned flow and artificially tripped flow have been investigated. Flow regions studied include the boundary layer and the near wake. Measurements were made at a free-stream Reynolds number based on airfoil chord of 1.25×10^6 and a free-stream Mach number of 0.1. Distributions of streamwise mean velocity, integral properties of the mean flow, turbulent intensities, and Reynolds shear stress are reported. For the naturally transitioned flow, the general trends observed are similar to those reported for a fully developed turbulent boundary layer over a flat plate under zero pressure gradient, with the exception of the notable streamwise variations in the turbulence properties for the airfoil flow. The main effect of flow tripping is to eliminate these streamwise variations. Observed changes in the mean-flow and turbulence fields caused by tripping are expected on the basis of the Reynolds number based on the boundary-layer thickness.

17. Key Words (Suggested by Author(s))	18. Distribution Statement
Turbulent boundary layer Turbulent wakes Airfoils Reynolds stress Incompressible flow	Unclassified - Unlimited Subject Category 34

19. Security Classif. (of this report)	20. Security Classif. (of this page)	21. No. of Pages	22. Price
Unclassified	Unclassified	42	A03

For sale by the National Technical Information Service, Springfield, Virginia 22161

NASA-Langley, 1981

4